Test Plan and Report

Over-voltage Protection of Direct Drive Wave Power System (WPS) Electrical Components

Awardee: C-Power

Awardee point of contact: Pukha Lenee-Bluhm

Facility: Cardinal Engineering, LLC

Facility point of contact: Doug Algera

Date: 04/24/2026

EXECUTIVE SUMMARY

The primary technical objective of this effort is to conceptually develop and optimize an over-voltage protection (OVP) system for the C-Power StingRAY™ Wave Power System (WPS). The work has been performed by assessing the conditions under which hydrodynamically induced transient over-voltage (OV) events occur, identifying means to detect these events, formulating and assessing solutions to mitigate their impact and protect embedded equipment, and performing a comparative analysis against the baseline to evaluate the impact on:

- Power Performance: percent improvement in annual mean electrical power (MEP) at PWS
- Capital expense: capital cost of OVP, increase over the base system
- Reliability: mean time to failure (MTTF) for the improved OVP system

To perform this comparative analysis, the proposed OVP system solution was compared against a baseline, an industrial standard design for emergency fault protection in wind turbines, which included a dynamic braking chopper (DBC) for DC link protection and a standard 3-phase remote operated circuit breaker for generator disconnect.

The C-Power StingRAY electric plant design was the basis for the over-voltage design investigation. The C-Power StingRAY performance data provided the original baseline for analysis. During the project, Cardinal Engineering analyzed MATLAB data provided by C-Power [1] and imported the data into a new and improved complete StingRAY electric plant model. The provided MATLAB data included hours of wave-induced generator velocity, power, and voltage which represented the StingRAY real seas performance at PacWave South (PWS). In this report, the MATLAB data will be referred to as PWS wave data. Accurate analysis of the performance data provided Cardinal simulation model validation, and ultimately the occurrence and frequency at which DC link over-voltages would occur for each scenario analyzed at PWS.

Over-voltages are of particular concern for this direct drive wave energy converter system because the system will need to be taken offline during impending overvoltage conditions, reducing the annual energy production. Reducing the number of over-voltage events is necessary to reduce risk and improve metrics of annual mean electric power production with fixed machine parameters. Current industrial solutions do not provide the target reliability or availability with consideration to the number of OVP annual events and recovery time. The maintenance of an OVP system is further complicated by the remote operating environment, making repairs difficult and costly. Over-voltage contingencies have the potential to cause extended outages when the generator output breaker opens, increasing downtime and reducing power production. The OVP is critical to protect the StingRAY electric plant, as failure modes of DC link due to over-voltage could be catastrophic. The OVP system was theorized as a combination of system designs; dynamic braking chopper (DBC), power flow control, flux weakening (FW), solid-state or other fast-acting switches, and controls, which would in combination create the performance, reliability and protection desired for a successful StingRAY WPS. Cardinal Engineering developed a detailed StingRAY electric plant simulation model which was used to assess different over-voltage protection (OVP) methods. The initial development of the more accurate model provided benefits over the StingRAY original baseline for analysis by the more accurate representation of the DBC and battery energy storage system (BESS) behavior and a more accurate representation of the active front end (AFE) rectifier. Beyond the new

improved StingRAY electric plant performance model, the most promising real seas operational OVP approaches, in addition to the built-in DBC and BESS, were found to be:

- An in-line fast-acting, long-lifetime disconnect switch to disconnect the permanent magnet generator (PMG) from the front-end inverters during times of impending over-voltage and rapidly reconnect it when the wave has subsided. The switch prevents over-voltage while avoiding the extended downtime that occurs when the PMG circuit breaker is tripped. We evaluated solid-state SCR-based solid-state disconnect switches and vacuum contactors. The solid-state switch does add power loss when compared to a mechanical switch. This power loss must be balanced against the reduced downtime that the solid-state switch provides as well as the discrete number of mechanical and electrical switching cycles that a mechanical circuit breaker can withstand.
- Flux weakening, or field weakening, to reduce the voltage induced in the stator by providing out-of-phase current, thus reducing the number of over-voltage events. Flux weakening is achieved by drawing a level of direct axis current (i_d), displaced 90 degrees from the nominal quadrature axis current (i_q), from the PMG into the active front end (AFE) rectifier. The current drawn at this angle creates a flux opposite to the electromotive force (EMF) produced in the stator by the permanent magnet rotor and hence reduces the PMG output voltage.

These methods, in combination with the DBC to ultimately protect the DC link and 3-phase remote operated circuit breaker to ensure disconnection in case of an OVP system fault contingency, can successfully improve all performance metrics within acceptable percentages.

To assess the effectiveness of the proposed OVP methods, Cardinal Engineering created a detailed MATLAB Simulink model of the StingRAY power system based on provided information and standard power system design practice. The model captures the overall StingRAY configuration and component parameters provided in the power plant design description document [2] and controls as described in [3], a spreadsheet describing generator output characteristics into the AFE over a range of generator speeds for different damping ratios. The generator, power converters, and other electrical components were modeled using standard Simulink components using parameters matching those of the StingRAY design. While reference [2] provides an overall description of the system operation and components, it did not provide enough information to develop detailed electrical models and control algorithms for all components. Where information was incomplete, Cardinal Engineering made assumptions based upon engineering judgement and industry standard design practices.

The power system model was then used to characterize system performance under two conditions:

- Sinusoidal generator speed input with a peak value of 10.1 to 12 RPM.
- Generator speed input from the PWS wave data [1].

Once the model was operating properly integrated and producing system behavior in accordance with the provided documentation, it was used to perform comparative design analysis of proposed OVP system approaches. The disconnect switch concept was tested by building a sub-scale version then exercising it against an emulated PMG output voltage. The test showed that impending over-voltage conditions could be detected and responded to in a rapid, repeatable manner. The schematic for the sub-scale disconnect switch and testbed is shown in Figure 1.

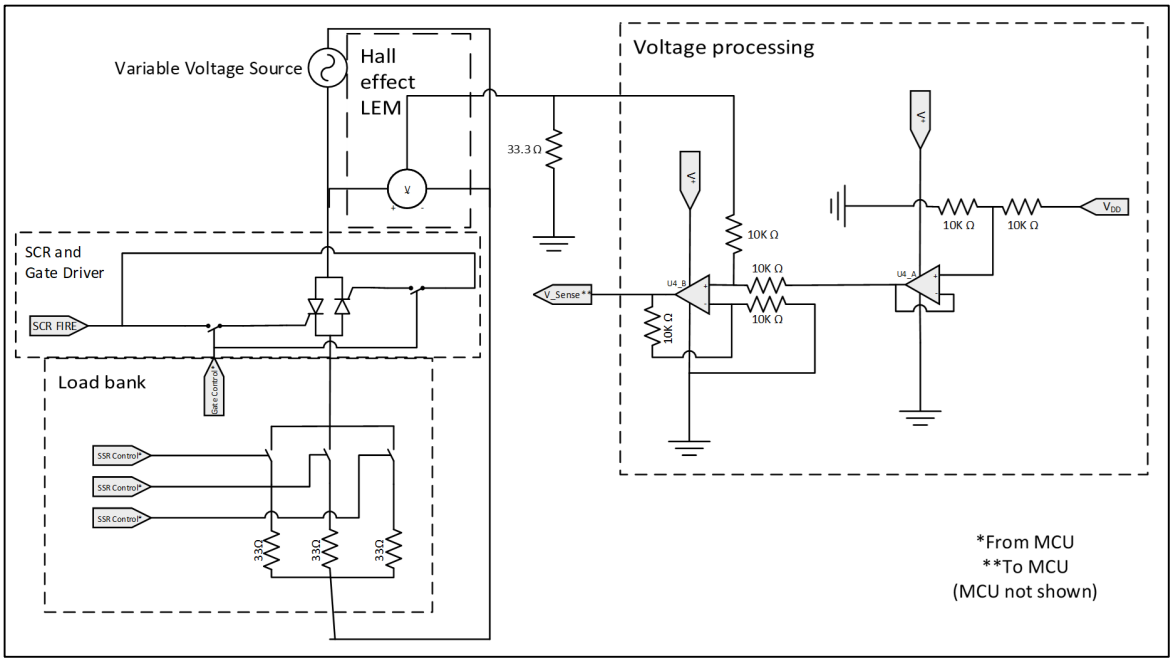

Figure 1. Single-phase sub-scale model of solid-state disconnect switch.

The original baseline performance parameters for the system were developed by performing a MATLAB analysis of the PWS wave data proved in [1] using a OV trip threshold of 7.61 RPM equating to a no-load generator voltage of 1.13 per-unit (PU) relative to the default DC link voltage (PU base value) at the default damping ratio. If gating is removed completely from the AFE, this would equate to a DC link voltage of 1.08 PU, allowing for the system to keep below the rated DC link overvoltage limit of 1.15 PU. The trip threshold of 7.61 RPM did not accurately account for voltage drops due to generator loading, DC link voltage management in real time through the use of the DBC, diversion of power into the BESS, nor output of power to the grid.

The new MATLAB Simulink model accounted for these effects as well as voltage drop across the generator, cables, and AFE rectifier input filter impedance, which lowered the AC voltage for a given speed and lowered the DC voltage relative to the AC voltage. When those factors as well as the OV mitigation methods were implemented into the new StingRAY electric plant model, we found that the trip threshold could be raised to 8.5 RPM for a less conservative trip threshold of 1.15 PU voltage. Flux weakening was demonstrated to further raise the maximum generator speed that StingRAY could withstand from 8.5 RPM to approximately 10 RPM. A plot showing the effects of flux weakening on simulated PMG output voltage is shown in Figure 2. In this instance, flux weakening delayed the over-voltage trip by 0.2 seconds for this particularly high RPM wave. In many instances, raising the trip level from 8.5 to 10 RPM avoids tripping altogether, reducing annual OVP events and increasing availability.

We assessed the effects of these increases in trip levels against the generator speed input from the PWS wave data. This analysis assumes that, once an over-voltage trip occurs, the PMG will remain disconnected from the AFE rectifier until the voltage decreases to less than 50V. Per Table 1, the annual number of trip events where the disconnect switch is activated to take the system offline reduces from 26,534 for the baseline case to 10,778 for the 8.5 RPM case. This is further reduced to 2,457 trips for the case with flux weakening (10 RPM).

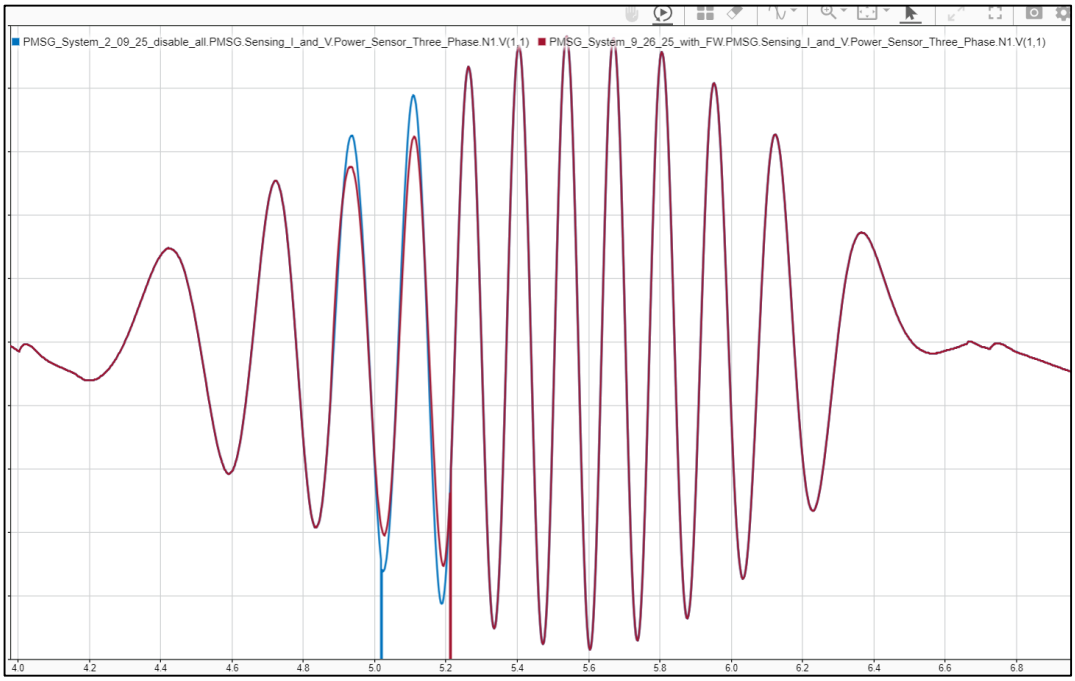

Figure 2. Reduction in PMG voltage due to flux weakening. Flux weakening in effect from 4.9-5.2 seconds, reducing peak voltage by >0.1PU.

Table 1. Number of DC link over-voltage trip events in PWS MATLAB wave data for baseline (7.61 RPM), model with DBC and BESS (8.5 RPM), and model with (10 RPM) flux weakening.

Dataset		7.61 RPM Trip			8.5 RPM Trip			10 RPM Trip		
	Dataset Percent Occurrence per year	Dataset number trip events	Dataset number trips/hour	Dataset number trips/year	Dataset number trip events	Dataset number trips/hour	Dataset number trips/year	Dataset Number trip events	Dataset number trip/hour	Dataset number trips/year
N7638cs3	1.51%	0	0.0	0	0	0.0	0	0	0.0	0
N7638cs9	6.45%	0	0.0	0	0	0.0	0	0	0.0	0
N7638cs15	3.28%	0	0.0	0	0	0.0	0	0	0.0	0
N7638cs21	0.20%	0	0.0	0	0	0.0	0	0	0.0	0
N7638cs27	14.07%	0	0.0	0	0	0.0	0	0	0.0	0
N7638cs33	2.74%	0	0.0	0	0	0.0	0	0	0.0	0
N7638cs39	13.19%	0	0.0	0	0	0.0	0	0	0.0	0
N7638cs45	16.29%	0	0.0	0	0	0.0	0	0	0.0	0
N7638cs51	8.14%	0	0.0	0	0	0.0	0	0	0.0	0
N7638cs57	0.28%	0	0.0	0	0	0.0	0	0	0.0	0
N7638cs63	3.16%	6	9.0	2496	2	3.0	832	1	1.5	416
N7638cs69	10.95%	0	0.0	0	0	0.0	0	0	0.0	0
N7638cs75	3.72%	0	0.0	0	0	0.0	0	0	0.0	0
N7638cs81	0.82%	39	58.6	4236	26	39.1	2824	2	3.0	217
N7638cs87	3.37%	12	18.0	5325	3	4.5	1331	0	0.0	0
N7638cs93	6.32%	2	3.0	1662	0	0.0	0	0	0.0	0
N7638cs99	0.56%	0	0.0	0	0	0.0	0	0	0.0	0
N7638cs105	1.54%	29	43.8	5923	13	19.6	2655	3	4.5	613
N7638cs111	1.65%	3	3.9	558	0	0.0	0	0	0.0	0
N7638cs117	0.42%	8	60.4	2250	5	37.7	1406	3	22.6	844
N7638cs123	0.76%	26	39.1	2590	9	13.5	897	3	4.5	299
N7638cs129	0.22%	2	2.3	43	0	0.0	0	0	0.0	0
N7638cs135	0.21%	9	54.1	1006	5	30.1	559	0	0.0	0
N7638cs141	0.15%	26	33.5	446	16	20.6	274	4	5.1	69
Total number trip events	100.00%			26534			10778			2457

Of course, the primary metrics of interest for wave power generation are annual mean electrical power and generated revenue. We performed analysis of the PWS wave data [1] to determine how implementation of the standard OVP mitigation methods of DBC plus BESS power flow (which raise the trip threshold to 8.5 RPM), flux weakening (which raises the trip threshold to 10 RPM), and the use of a fast-acting disconnect switch affected the annual mean electrical power as compared to the baseline case where the system trips at 7.6 RPMs and remains offline for at least 30 seconds and as compared to the ideal situation where no trips occurred. Assumptions for this analysis were as follows:

- The fast-acting disconnect switch, once opened due to an over-voltage event, would remain offline until generator voltage dropped below 50 volts, at which point it would reclose.
- The conventional mechanical circuit breaker, once opened due to an over-voltage event, would remain offline for 30 seconds to allow for spring recharging and reclosing at a trough in output voltage.
- Loss characterization of the solid-state disconnect switch was based upon a two-leg implementation [4] of antiparallel Hitachi/ABB 5STP2800 thyristors [5]. This design and the loss calculations will be described in greater detail later in this report.

- The analysis does not account for downtime for maintenance or other unscheduled outages and their impact on the mean-time-to-failure (MTTF) of the system. Each loaded switching event for a conventional mechanical circuit breaker takes life out of the breaker. The downtime to replace or repair a worn out circuit breaker would reduce delivered energy far more than the 30-second interruptions to reconnect to the system. Additionally, every over-voltage event poses a risk to damage components connected to the DC link, particularly DC link capacitors.

The different scenarios are compared to determine how much energy capture is lost due to over-voltage trips with and without built-in OVP mechanisms (DBC, BESS), with and without flux weakening (FW), how much is lost when accounting for 30 second downtime with a conventional breaker, and how much is lost due to solid-state disconnect switch conduction losses. Results are shown in Table 2.

Comparing the results from the different OVP methods to the 7.6 RPM trip threshold baseline, we get the following percent improvements in annual MEP:

- Increasing the trip threshold to 8.5 RPM via DBC and BESS results in a 3.12% increase in MEP versus baseline.
- Further increasing the trip threshold to 10 RPM via FW results in a 5.41% increase in MEP versus baseline.
- Incorporation of a low-loss, fast-acting disconnect switch raises the MEP advantage over baseline for the 10 RPM case to 5.76%
- If the fast-acting disconnect switch is solid-state, the advantage over baseline lowers to 4.71%.

Notable observations from this table regarding comparison to the ideal case with no over-voltage trips:

- The baseline case, with its low trip threshold and 30 second downtime, results in an annual mean electrical power (MEP) reduction of 5.77% versus the ideal case with no trips.
- Simply raising the trip threshold to 8.5 RPM lowers the reduction versus ideal to 2.83%.
- Further raising the trip threshold to 10 RPM via flux weakening changes the reduction versus ideal to 0.68%.
- Implementation of a low-loss fast-acting disconnect switch without conduction losses that reconnect the PMG to the AFE rectifier at an AC voltage less than 50V reduces losses versus ideal to 0.08%.
- If the fast-acting disconnect switch is a solid-state SCR-based switch, losses versus ideal increase to 1.33% with FW. Solid-state disconnect switch SCR losses alone are approximately 1.26% of the ideal delivered energy.

Table 2. Assessment of energy losses versus baseline and ideal due to overvoltage trip downtime and SCR losses

runName	Dataset Percent Occurrence per year	Case 1. Ideal All Energy Available	Case 2. Baseline (7.61 RPM) with 30 s recovery	Case 3. 8.5 RPM, 30s recovery	Case 4. 10 RPM (FW),30s recovery	Case 5. 10 RPM (FW), 50V recovery	Case 6. 10 RPM (FW), 50V recovery with SCR losses
		MEP	MEP	MEP	MEP	MEP	MEP
N7638cs105	1.54%	2.34E+05	1.62E+05	1.90E+05	2.22E+05	2.33E+05	2.31E+05
N7638cs111	1.65%	1.25E+05	1.21E+05	1.25E+05	1.25E+05	1.25E+05	1.24E+05
N7638cs117	0.42%	2.27E+05	1.51E+05	1.74E+05	1.95E+05	2.22E+05	2.20E+05
N7638cs123	0.76%	2.01E+05	1.54E+05	1.77E+05	1.94E+05	1.99E+05	1.98E+05
N7638cs129	0.22%	1.47E+05	1.44E+05	1.47E+05	1.47E+05	1.47E+05	1.45E+05
N7638cs135	0.21%	2.32E+05	1.49E+05	1.76E+05	2.32E+05	2.32E+05	2.30E+05
N7638cs141	0.15%	2.03E+05	1.49E+05	1.69E+05	1.93E+05	2.01E+05	2.00E+05
N7638cs15	3.28%	1.59E+04	1.59E+04	1.59E+04	1.59E+04	1.59E+04	1.54E+04
N7638cs21	0.20%	6.15E+03	6.15E+03	6.15E+03	6.15E+03	6.15E+03	5.79E+03
N7638cs27	14.07%	4.81E+04	4.81E+04	4.81E+04	4.81E+04	4.81E+04	4.72E+04
N7638cs3	1.51%	3.65E+04	3.65E+04	3.65E+04	3.65E+04	3.65E+04	3.57E+04
N7638cs33	2.74%	1.22E+05	1.22E+05	1.22E+05	1.22E+05	1.22E+05	1.21E+05
N7638cs39	13.19%	9.84E+04	9.84E+04	9.84E+04	9.84E+04	9.84E+04	9.72E+04
N7638cs45	16.29%	6.39E+04	6.39E+04	6.39E+04	6.39E+04	6.39E+04	6.29E+04
N7638cs51	8.14%	3.76E+04	3.76E+04	3.76E+04	3.76E+04	3.76E+04	3.68E+04
N7638cs57	0.28%	1.98E+04	1.98E+04	1.98E+04	1.98E+04	1.98E+04	1.93E+04
N7638cs63	3.16%	1.79E+05	1.59E+05	1.72E+05	1.74E+05	1.79E+05	1.77E+05
N7638cs69	10.95%	1.25E+05	1.25E+05	1.25E+05	1.25E+05	1.25E+05	1.24E+05
N7638cs75	3.72%	5.75E+04	5.75E+04	5.75E+04	5.75E+04	5.75E+04	5.66E+04
N7638cs81	0.82%	2.40E+05	1.46E+05	1.70E+05	2.34E+05	2.40E+05	2.38E+05
N7638cs87	3.37%	1.84E+05	1.53E+05	1.73E+05	1.84E+05	1.84E+05	1.82E+05
N7638cs9	6.45%	2.84E+04	2.84E+04	2.84E+04	2.84E+04	2.84E+04	2.78E+04
N7638cs93	6.32%	1.19E+05	1.13E+05	1.19E+05	1.19E+05	1.19E+05	1.18E+05
N7638cs99	0.56%	7.85E+04	7.85E+04	7.85E+04	7.85E+04	7.85E+04	7.74E+04
Annual MEP		8.64E+04	8.15E+04	8.40E+04	8.59E+04	8.64E+04	8.53E+04
MEP increase versus Baseline		+ 6.13%	+ 0.00%	+ 3.12%	+ 5.41%	+ 5.76%	4.71%
MEP decrease versus Ideal		- 0.00%	- 5.77%	- 2.83%	- 0.68%	- 0.08%	- 1.33%

Raising the trip threshold to 10 RPM via the addition of flux weakening, by reducing the number of circuit breaker trips, also greatly improves system MTTF. If the circuit breaker is rated for 5,000 loaded operations, a typical value for loaded switching operations, the number of failures is reduced from 5.3 to 0.49 times per year. Most circuit breakers are rated for fewer loaded operations than this. If the circuit breaker is replaced with a long-life disconnect switch, such failures will be nearly eliminated given the very long life of solid-state switches and vacuum contactors. MTTF will also be improved by reducing exposure of system components to overvoltage events in general.

The improved MTTF and additional energy delivered must be balanced against the cost of implementing the improvements. We do not have a cost for implementing flux weakening. This would have to be integrated into the AFE rectifier controls by the OEM. We estimate the cost of the solid-state disconnect switch to be between $30,000 and $50,000. We estimate the cost of the vacuum contactor-based

disconnect switch to be approximately $16,000. These costs are trivial in the context of the overall cost of the system.

Conclusion:
Improvement in real time DC link voltage management is necessary to minimize OV events and reduce risk to components connected to the DC link, specifically electrolytic capacitors. In practice, DC link voltage regulation between multiple inverter power sources, the generator and BESS power converters, can be achieved with advanced high-speed real-time control loops, such as PROFINET, an industrial standard for real-time communications. Modeling showed that built-in approaches to OVP, namely the DBC and BESS, can raise the trip threshold versus baseline from 7.6 RPM to 8.5 RPM, greatly increasing MEP. The modeling effort found two additional viable approaches to OVP, flux weakening and the use of a solid-state or other fast-acting disconnect switch, that further improve annual MEP and MTTF to completely fulfill the original project goals.
The primary lesson learned was that having a functional simulation model enables exploration of a number of different OVP approaches. It is recommended that both proposed approaches – an SCR-based or other fast-acting switch to quickly and reliably disconnect and reconnect in response to an OV event, and flux weakening to reduce induced voltage and delay or avoid an OV event – be applied to the StingRAY design, in addition to optimizing built-in systems such as the DBC and BESS.

1. INTRODUCTION TO THE PROJECT

The primary technical objective of this effort is to conceptually design, develop and optimize an over-voltage protection system for the C-Power StingRAY™ Wave Power System (WPS), by assessing the conditions under which hydrodynamically induced transient over-voltage events occur and identifying means to effectively detect and quickly respond to these events to protect the system and ensure maximum up time. This is accomplished by formulating and assessing solutions that mitigate the impact of over-voltage events and protect embedded equipment, and then further developing a select economic solution that improves annual power production, increases availability and reliability.

As described in reference [2], C-Power's StingRAY WPS is a floating, two-body structure (see Figure 3) designed to provide utility-scale power for offshore applications and terrestrial grids. The StingRAY nacelle houses a power take-off (PTO) featuring a large diameter, direct drive rotary permanent magnet generator (PMG). The PMG rotor is connected to the float, while the stator is fixed to the nacelle. Thus, the PTO is actuated by the relative pitching motions of the float and nacelle. These wave driven rotational speeds are typically less than 1 to 2 revolutions per minute (RPM) but can infrequently peak upwards of 20 RPM. The voltage output of a PMG is directly correlated to several factors including winding configuration, machine form factor and composition, and shaft rotational speed. Since the velocity of the float varies throughout the motion of a single wave and since waves vary in duration, height, and shape; the voltage developed has widely variable voltage magnitude and frequency.

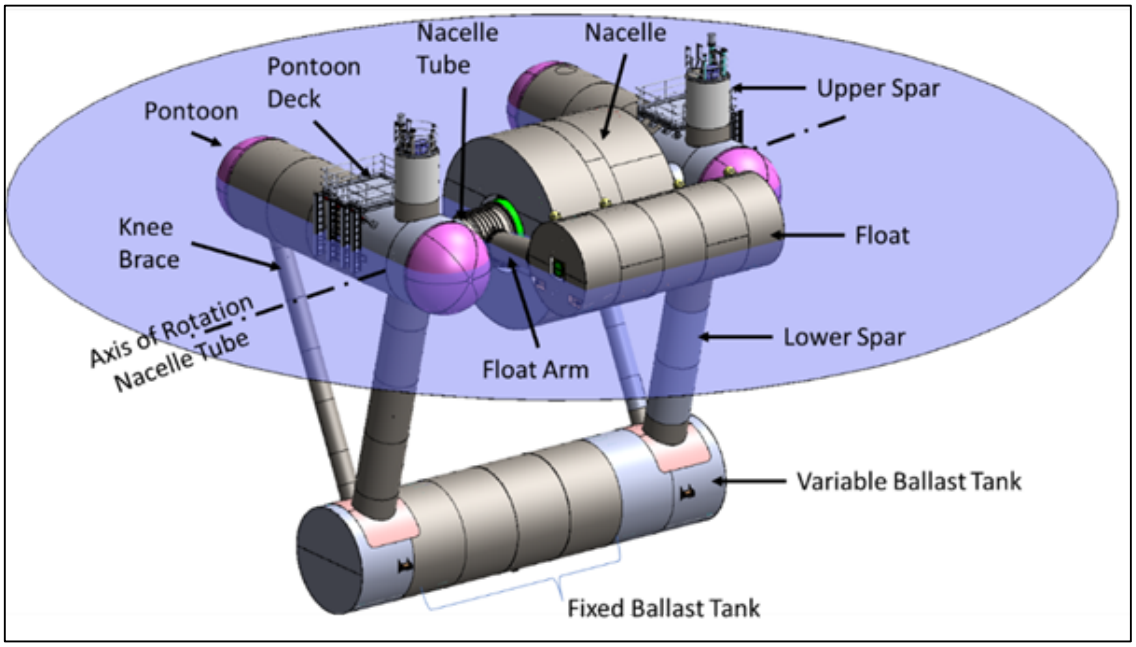

Figure 3. StingRAY general arrangement.

To utilize this highly variable voltage and frequency, the output of the PMG is fed into parallel active-front-end (AFE) rectifiers of a commercial low voltage drive, which rectify the output to controlled direct current (DC) bus [2]. This bus is used to manage energy storage and feeds an inverter that connects to the alternating current (AC) grid through a step-up transformer. Per [2] the DC bus also has interfaces to a battery energy storage system (BESS) and braking resistor through DC-to-DC converters (see Figure 4). The DC-to-DC converter feeding the braking resistor is referred to as the dynamic braking chopper (DBC).

C-Power characterized the wave motion at the expected citing location for StingRAY and optimized the performance of the generator while minimizing the number events that would result in over-voltage conditions within the LV3 drive system, notably limiting the times the DC link would exceed its maximum voltage limit. Designing for over-voltage events was determined to be necessary to optimize the efficiency of the direct drive energy conversion system, generator, power electronics, and energy storage.

The design environmental conditions for this effort are based upon the PacWave South (PWS) test site. PWS is an in-development, state-of-the-art, pre-permitted, accredited, grid-connected wave energy test facility developed in partnership with the US Department of Energy, the State of Oregon, and the local community. The test site, which comprises four berths, is located 12 km offshore of the Port of Newport and encompasses nearly 7 sq. km.

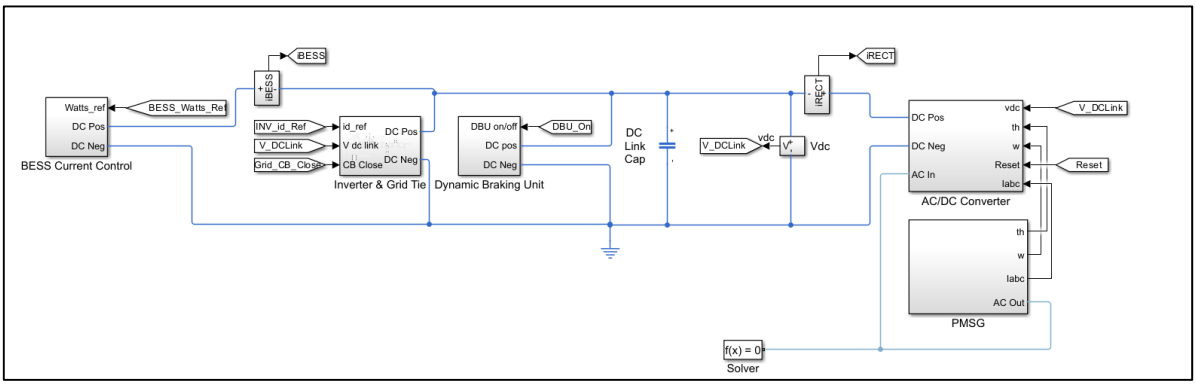

Figure 4. StingRAY Single-line Diagram.

C-Power conducted a wave resource characterization for PWS (referred to in this report as PWS wave data), based upon data from a 32-year, high-resolution hindcast created by Pacific Northwest National Lab (PNNL) and made available by National Renewable Energy Lab (NREL). The expected annual occurrence of sea states, characterized by significant wave height (Hm0) and energy period (Te), is depicted in the occurrence table shown in Figure 5. The color of each bin, and the number within, indicate the relative rate of occurrence (parts per 10,000) in an average year.

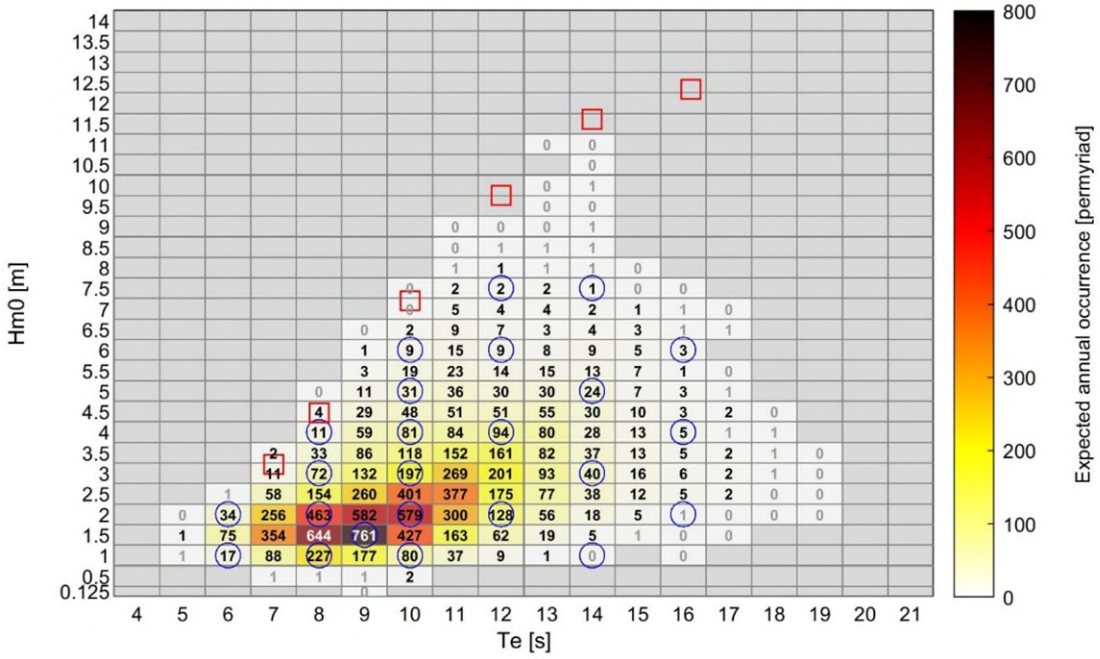

Figure 5. Expected Annual Occurrence Rates of Sea States at PacWave South.

The expected behavior of the StingRAY WPS, including the direct drive PMG voltage oscillations, will be determined via numerical simulations in sea states representative of operational and extreme conditions. Note that the direct drive rotary PMG voltage output is linearly proportional to the wave-driven shaft speed (or rather, the shaft speed with respect to nacelle speed) and oscillates between zero and a local

peak with every wave half-cycle, typically crossing zero-speed twice every 3 to 15 seconds. To reduce the number of simulations required, a subset of sea states will be considered in this investigation. Conditions that are reasonably expected to occur on an annual basis will be represented by a subset of 24 operational sea states (OSS), as indicated by the blue circles in Figure 5. Annual occurrence rates were calculated for each of the 24 OSS, assuming that these 24 sea states represent the annual wave resource, based upon the distance (in Hm0-Te space) of each instance in the 32-year hindcast to the center of the 24 selected bins. A subset of six extreme sea states (ESS) was selected for consideration, from points along the 50-year return environmental contour and are indicated by red squares in Figure 5. Analysis time for the OSS was a minimum of 40 minutes, or 200 times the energy period (Te), whichever was greater. Note that the nominal analysis windows were trimmed at both ends to the nearest voltage zero-crossings. In a few cases, additional data was discarded to exclude unreasonable data from analysis, therefore each data set total evaluated time varied and was weighted accordingly.

Analysis of OSS simulation results under the baseline design assumptions identified a total of 119 over-voltage events in the 24 data sets, for an estimated occurrence rate of 26,534 events annually. For the baseline an over-voltage event is defined as 1.13 PU voltage, based on a no-load back-emf from the generator, which correlated directly to 7.61rpm. For the results based on the complete electric plant MATLAB simulation, overvoltage events are defined as the point at which the DC-link voltage reaches 1.135 PU, which is has less margin to the design limit of 1.15 PU.

Typically OV events last less than a second, as the wave-driven shaft oscillation momentarily crosses the corresponding speed threshold. Eleven of the twenty-four OSS have at least one OV event per hour, with rates falling between 2 and 60 OV events per hour. These eleven sea states account for roughly 19% of the average year (on the basis of 24 representative sea states). In the baseline design as described in [2], a conventional mechanical air circuit breaker was used to isolate the AFE rectifiers of the electric plant from OV conditions at the generator output. Due to the time for the circuit breaker motor to charge the closing springs, the air circuit breaker may take up to a minute before the system can be brought back online. To make matters worse, the standard air circuit breakers used in baseline design have a service life on the order of 1,000 to 7,000 electrical operations, acceptable for wind turbines, but for direct drive wave energy, it would fail in 2 or 3 months in expected conditions, far less than the targeted 20-year life of the system. The baseline circuit breaker protection system, as justification for this project, accentuates the need for a proper commercial solution for an OVP system.

By way of example, Figure 6 presents characteristics of the OV events from one of the 24 OSS simulations, namely: the number of events, their peak voltages, and the elapsed event times[1] (above the threshold). While the sea state in this example (oss21: Hm0=6m and Te=12s) isn't common, accounting for 0.76% annual occurrence on the basis of 24 representative sea states, the 26 OV events indicate an average rate of 39.1 events per hour, and result in an estimated 2,590 events annually. In this particular simulation, the average time between over-voltage events is 77s, although there are instances of 3 or more events in less than a minute.

[1] Event time – Elapsed time the simulation resulted in voltage production greater than the allowed system voltage. Use to represent the scale of time where an over-voltage condition exists within the operations of the current system design.

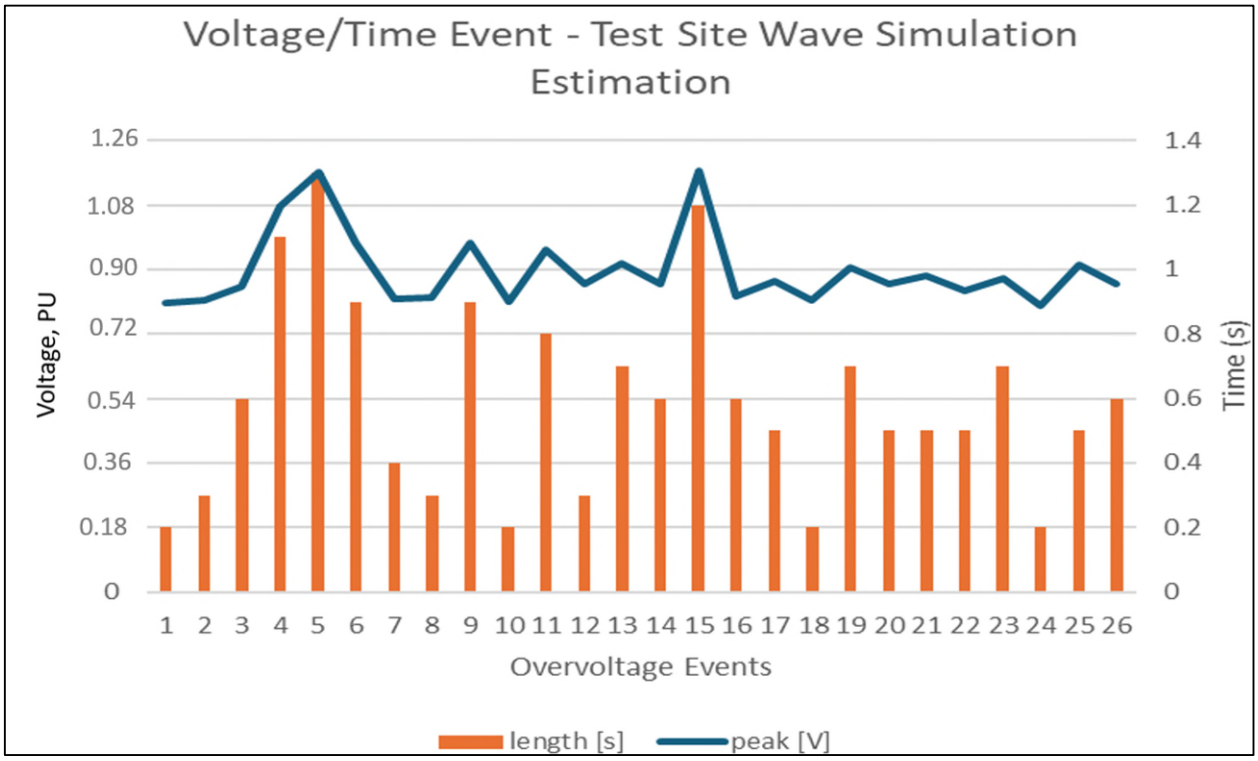

Figure 6. Over-voltage Events from C-Power Simulation of Operational Sea State (ID oss21)

StingRAY detailed electrical design description and assessment

The use of an ultra-low speed PMG is quintessential to efficient direct drive wave energy conversion. However, unlike a wound field generator, there is no way to modify the magnetic field strength of the rotor of a PMG. This means that the open-circuit output voltage will be directly proportional to rotor velocity, which is determined by wave external forces (i.e. wave action). During normal wave actuations of the direct drive generator, the pulsed voltage output of the PMG may be high enough that the active front end (AFE) rectifier of the drive system will not be able to regulate the DC link properly, resulting in an over-voltage condition on the DC link. This is the reason for this OVP design and analysis.

The AFE is a standard two-level three-phase converter using Insulated-Gate Bipolar Transistors (IGBTs) as switching devices. Even if the IGBT gate signal is removed completely, the anti-parallel body diodes of the IGBTs will still conduct when forward biased so that the AFE will look like a diode rectifier when the gate signal is removed. The DC output of a three-phase diode rectifier is ≈1.35 times the root mean square (RMS) value of the AC input voltage, so any AC output voltage above 1.20 PU would result in the DBC sending a trip signal to the circuit breakers between the PMG and the AFE even if the gate signal was removed from the IGBTs unless there were other means to regulate the DC link. For practical reasons, the trip threshold would be set lower than this to provide headroom between the time the trip is issued and the voltage level at which damage can occur. Reference [1] suggests a cutout voltage of 1.09 PU on the AC side. (Note: the DBC is designed to mitigate DC link over-voltages by dissipating energy to discharge the DC link capacitor, but the level of energy dissipation is limited by the maximum duty cycle limit of the braking resistors. Braking choppers typically dissipate energy from regeneration of a motor fed by the

drive and are therefore limited in how much energy they can dissipate.) Whereas the baseline DBC and PMG circuit breakers are a necessary industry standard solution for circuit protection in the case of a fault, opening the PMG circuit breaker on a semi-regular basis for over-voltage transients is unacceptable for several reasons:

- Reclosing the breaker may require manual intervention, which takes the system offline for an extended period of time, resulting in loss of generating capacity.
- Mechanical breakers and contactors have a limited number of close and open cycles. The number of loaded open cycles is not listed in [2] but will be significantly less than the no load cyclic rating due to arcing of the contacts. Typical numbers of loaded electrical operations for air circuit breakers are 1000-7000 operations.
- The speed at which mechanical air circuit breakers open upon command is slow, meaning that once a pending over-voltage condition is detected, the delay between the command to open and the actual opening could potentially allow DC link voltage to rise to destructive levels.

Cardinal Engineering was tasked with investigating and developing solutions to wave-driven over-voltage conditions that did not involve opening the input circuit breaker. In order to do this, a detailed StingRAY electric plant simulation model was developed. The model was implemented using the MATLAB/Simulink Simcape Electrical blockset. This report describes the model, provides results for different mitigations, and makes recommendations regarding the preferred mitigation approach.

2. Roles and Responsibilities of Project Participants

2.1 Applicant Responsibilities and Tasks Performed

C-Power will provide the baseline WPS design, including architecture and characteristics of the generator, electric plant, and legacy over-voltage protection system. C-Power will be responsible for:

- Determining WPS hydrodynamic operational response (e.g., shaft speed, power and voltage out of the generator) in sea states representative of the wave resource at PWS, utilizing ANSYS AQWA for hydrodynamic simulations.
    - C·Power will work with Cardinal Engineering to identify / characterize a subset of transient over-voltage events from the simulation data, useful for assessing alternative OVP systems.
- Determining WPS performance in specified sea states, and average annual power at PWS, using baseline and alternative design(s).
- Characterization of capital expense, reliability, and availability for the baseline design.
- Providing an engineering specifications package for the baseline design with pertinent information for the OV system design, including electrical diagrams, specifications for the rotating machine (winding configuration, current ratings, pole location, etc.), specifications for all interconnected electrical components that include voltage and current ratings.

2.2 Network Facility Responsibilities and Tasks Performed

Cardinal Engineering will be responsible for:

- Reviewing and evaluating the transient over-voltage events identified by C-Power from their StingRAY hydrodynamic simulation results.
- Conducting electrical engineering analysis of identified hydrodynamically induced electrical transients to identify and characterize over-voltage protection (OVP) concerns for direct drive WPSs and specific components of interest.
- Developing a list of critical components and their corresponding voltage thresholds.
- Conducting statistical analysis of simulation data and determining the optimal target for maximum operating voltage to minimize down-time due to voltage conditions that exceed electrical equipment ratings.
- Assessing the simulation data provided by C-Power.
- Survey several commercially available over-voltage protection hardware options based on components identified (hardware, sensors, and control methodologies) and assessing how they might be employed on WPS. This analysis will incorporate a balance of plant assessment, a study to determine uniqueness of the solution, and will use net power output as the primary optimization metric. Example solutions will include:
    - Active response local energy storage and power conversion components.
    - Passive response voltage clamps or crowbar circuits.
    - Solid state switching circuit interrupt or insertion, considering hybrid circuit breaker incorporation.
    - Flux weakening controls schemes to limit generator output.
- Conducting an assessment of control systems utilized in terrestrial microgrids, wind conversion equipment, and shipboard power systems to introduce legacy options for dynamic over-voltage protection without negatively impacting WPS performance.
- Development of conceptual OVP design solutions for the StingRAY WPS and assessing the benefits and risks of proposed alternative over-voltage control methods against the baseline design.
- Perform statistical analysis of the OV events based on design limits of solutions to evaluate performance parameters, such as MTTF (mean time to failure). Investigate and quantify the quality of proposed design solutions that have been developed based on parametric analysis of OV events for each solution.
- Down select solutions based on optimization of performance metrics, and secondary parameters. Recommend and report performance metrics for the best solution to C-Power.

3. Project Objectives

The primary objective is to increase the overall power production capability of wave energy devices through the design and/or control systems that can be incorporated into electrical system designs that enable the system to rapidly recover power generation during periods in which high speed events cause induced voltages beyond the limitations of the electrical system's ratings. Whereas typical over-voltage protection systems disconnect and remain off-line, the goal of this project would be a fast-response over-

voltage protection and recovery system which maximizes available up-time during frequent over-voltage events.

The C-Power electrical baseline design is a conventional air circuit breaker-operated over-voltage protection system where the power production generator voltage, is physically isolated from the power electronics and power connection to the grid. During any over-voltage event, the protective feature of the electrical system is to disconnect the power generation from the electrical system. The system restores after a defined period of time which disables the StingRAY from power production during that same period of time. Because power is not converted during these mechanically energetic periods, the mean annual power generated is lowered, which is seen as a reduction in total system net power output based on the incident wave power. The goal is to capture a larger percentage of the available power during these events.

The following optimization impact metrics will be estimated, and compared to the baseline StingRAY design, to evaluate the impact of the proposed solutions:

- Power Performance: percent improvement in mean annual electrical power at PWS
- Capital expense: capital cost of OVP, increase over the base system
- Reliability: mean time to failure (MTTF) for the improved OVP system

Cardinal Engineering and C-Power intend to publish the findings of this effort and present at an upcoming technical conference such as the National Hydropower Association's (NHA) Waterpower Week or University Marine Energy Research Community (UMERC) (specific conferences are to be determined based on analysis progress relative to submission deadlines). While C-Power may reserve certain StingRAY-specific design details that are commercially sensitive but not covered under existing patents, analysis methods developed through this study and their impacts on the StingRAY case study will be thoroughly documented and made available for public distribution through the post-access report.

4. Test Facility, Equipment, Software, and Technical Expertise

Cardinal Engineering, a small business headquartered in Annapolis, Maryland, provides a broad range of engineering services in the marine industry, to government and commercial clients. Cardinal Engineering is the incumbent design contractor for the StingRAY WPS hull systems and is also familiar with International Electrotechnical Commission (IEC) technical specifications and DNV methodologies and calculations which are the governing specifications of the WPS.

Cardinal Engineering's Linwood PA facility consists of approximately 1400 sq. ft. of laboratory high bay space and 1700 sq. ft. of office space. The Linwood facility is served by 400 amps of 208 VAC, 3 phase power and is representative of a typical commercial setting. Within the facility Cardinal Engineering has all the necessary tools to support manufacturing including incoming inspection, controller fabrication, cable termination, enclosure assembly and functional testing. The facility is currently being used to develop and test a rapidly deployable microgrid for the United States Air Force. Assets in the lab include

a diesel-powered MEP-803 10kW three phase military generator, and hardware to support a demonstration of the microgrid. These assets are available for use in the testing effort as needed.

Cardinal Engineering power system engineers will use MATLAB and various MATLAB toolboxes such as Simulink, Simspace Power and the Statistics and Machine Learning toolbox to evaluate the C-Power provided WPS data. Models and algorithms developed during this analysis can be applied in the laboratory environment to representative controller hardware.

Cardinal Engineering's laboratory capability will be enhanced with select Controller Hardware in the Loop (CHIL) purchases during the scope of this effort. This includes a Programmable Logic Controller (PLC) backbone, input / output (I/O) module hardware, data acquisition capability, and the required OVP concept hardware (or functional equivalents) to develop a CHIL test bed for the solution or solutions.

5. Test or Analysis Article Description

Simulation data from the C-Power power generation to electric distribution was evaluated to identify over-voltage conditions and develop performance statistics of the proposed designs based on operational voltage limits. This analysis was based on C-Power's simulation data of the StingRAY hydrodynamics and the direct drive permanent generator at PWS combined with a detailed model of the StingRAY overall electric plant in MATLAB Simulink. The analysis determined system performance indicators and parameters for OVP design comparison, such as increased power production and availability, as well as component analysis for reliability and cost.

The intended purpose is to create an over-voltage protection design criterion for all wave energy converter applications, a potential initial guideline for a standard for a fast-recovery over-voltage protection design, and more specifically to develop a design that will work for the C-Power StingRAY WPS. The success of this analysis, design, and testing will theoretically pave the way for future direct drive generator and power electronic designs by setting an example of best practices and methods of design for dealing with over-voltage conditions on wave power systems.

The analysis of the voltage time history from real seas simulations was used to determine typical event indication time periods with respect to the sea climates, typical lengths of overvoltage conditions, and indicators within the system that can be used to provide indications to algorithm(s) or control systems to enable actions to minimize overvoltage conditions. This analysis was performed by delineating the real seas information into two distinct, not mutually exclusive, protection schemes:

Normally operating over-voltage suppression – This protection mechanism works to reduce the operating voltage of equipment during regularly occurring events, increasing system uptime by reducing the duration of circuit interruption.

Emergency operating over-voltage suppression – This protection mechanism functions in the event of extreme outliers in operation or faulted conditions. The protection schemes employed in these scenarios will interrupt the circuit to protect equipment in uncommon events. In these scenarios the output power

of the system is not considered to be a pivotal component in the analysis and is focused primarily on protecting the WPS device and its electrical generation powertrain.

Define associated power conversion (wave energy to electrical energy) events that will trigger an overvoltage event. Goal of the analysis was to determine typical event indication time periods (time of energy conversion just prior to overvoltage event), typical lengths of an overvoltage condition, and indicators within the system that can be used to provide indications to algorithm(s) or control systems to enable actions to minimize overvoltage conditions.

Create an algorithm that uses the C-Power simulation data of real seas, real time voltage, and parameters established by design concepts, to identify best methods of measurement and reaction time requirements.

Using the above algorithm(s) and information from simulations - develop potential control system(s) and OVP concept design(s) which could potentially improve the performance metrics.

Upon completion of the control(s) and OVP system design(s) – develop a simulation of the hardware and apply test scenarios to the model(s) which verify system response. Implement controller I/O as applicable based on the target design.

Coordinate with C-Power and apply PWS test data on profile to determine power output gain by utilizing control algorithm and control scheme.

6. Work Plan

6.1 Experimental Setup, Data Acquisition System, and Instrumentation

Four potential design concepts were evaluated in this effort. These notional systems are described below:

1) *Active Component Response* – A condition-based controller will collect data from the environment and use a series of internal logic controls to implement a hardware solution that may include power conversion, energy storage, energy diversion, or energy dissipation mechanisms.
2) *Passive Component Response* – The utilization of analog devices will be explored to create a passive voltage suppression solution. This would eliminate the requirement for an embedded logic control which would potentially decrease response time, but may limit the overall system functionality, future flexibility, and potentially system agnostic application.
3) *Transient Solid-State Switching* – The advent of solid-state switching devices and hybrid overcurrent protection breakers may enable more dynamic response of interruption methods, limiting equipment downtime on the order of seconds vice minutes. This is an adaptation of the legacy method but with rapid response capability with limited hardware modifications may provide the required benefit while limiting complexity.
4) *Rotating Machine Manipulation* – Advanced control techniques on the prime mover can decrease voltage potential by flux weakening regimes. Important analyses in this technical area

will include compatibility of winding configurations and the current source and power conversion equipment required to back feed the windings. Other concepts, like dual wound machines, can be explored to expand the trade space if this is determined to be an optimal solution set.

The following steps will progressively advance the design using the activities shown in Figure 7. These steps are described in more detail in the following paragraphs.

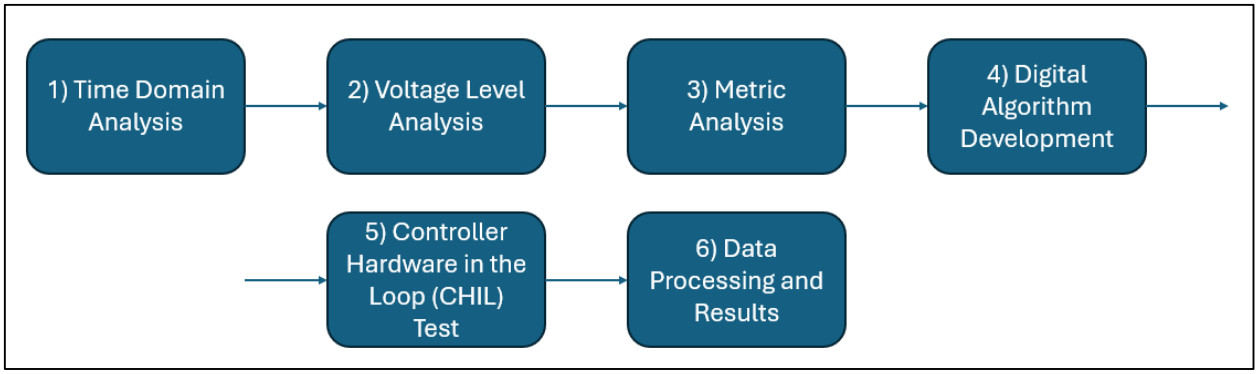

Figure 7. Incremental progression of over-voltage protection hardware and software development.

First, the most important characteristic to define for each concept is the time scale required for response, activation, and deactivation of the voltage suppression mechanism. This will be critical to define the sensor suite, data requirements, processing bandwidth, and ultimately the overall system benefit. These concept solutions will be individually evaluated against the legacy system using simulated operational data to illustrate the potential functionality and the overall operational benefit (e.g., net power output).

Another important parameter to consider is the target value for the over-voltage suppression mechanism. This will be driven by the component ratings inherent to the system design and the amplitude and magnitude of over-voltage events in the current system. The power conversion system (PCS) damage is the primary consideration here and will set the upper limit thresholds. Next, the simulation data will be analyzed to determine the optimal voltage target for the suppression device by balancing the net power output of the baseline solution with the amount of energy saved during the over-voltage mitigation method implementation. If the initial time domain and voltage level analysis determines that one of the options is not feasible, then it will be eliminated from consideration.

With the time scale and voltage level determined, notional components will be selected for each option. Each conceptual design will be the basis for an analysis across the following parameters (which expand upon the primary optimization impact metrics first listed in Section 3):

- Volume and mass envelopes
- Required interfaces
- Component Cost
- Net power output (gains/losses)
- Reliability
- Emergency condition operation

- Failure impacts
- Impact on the plant during normal operation
- Cross compatibility with other wave energy converters
- Power quality impacts

Once these parameters have been characterized, the conceptual design can be further evaluated in the digital space. This analysis leveraged the data output from the power simulation and add functionality that imparts the impact of the voltage suppression device. This includes developing an algorithm using regressive data analysis that predictively activates the device when a series of conditions are met. Once this algorithm is developed, it will be tested on simulated data in digital space. Important outputs from this simulation are false-positive triggers, and events that fail to trigger the device. The impacts of both will be categorized and documented to ensure improvements on the algorithm are captured.

To further illustrate the feasibility of the various solution sets, a scaled Controller Hardware in the Loop (CHIL) test bed will be established. A diagram of this system is shown below in Figure 8.

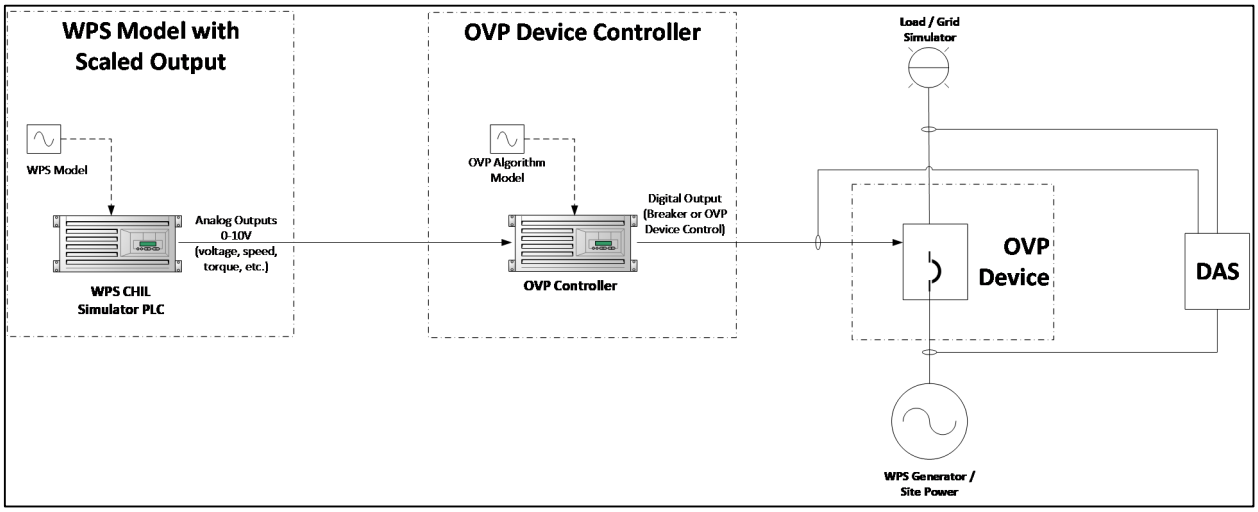

Figure 8. CHIL Test Bed for OVP Device.

Here a signal generator will replicate the performance of the wave generator model and feed this data into a PLC based controller that is running the previously developed control algorithm. Run time speeds for the proposed hardware set up are dependent on the models, the modeling and simulation computer's performance and the PLC's response times. To demonstrate full system capability, in real time, more advanced real time simulation hardware is required, which is outside the scope of the proposed work. The control algorithm will activate based on a series of input parameters and will output a response variable to control a solid-state relay (or functional equivalent). This functionality can be mapped in real-time over the simulated data to demonstrate effectiveness of the proposed solution and the ability of a PLC to operate at the time scale required for an effective response.

C-Power provided the PWS wave data to Cardinal Engineering in MATLAB format. Cardinal Engineering analyzed the simulation data and subdivided it into event specific data packs. Relationships between the

measured parameters were identified as event indicators for mitigation methods. These efforts were done with MATLAB and associated MATLAB toolboxes.

MATLAB will be set up to provide data samples based on the mitigation methods to provide average efficiencies based upon the mitigation method chosen. This data run will change the overall system net power output for the data sample. This will be repeated for each mitigation method.

Results from the mitigation methods were evaluated against the baseline of the current electrical system design response for the StingRAY. Once a series of data samples and mitigation methods are created and results collected, the Cardinal Engineering team will document changes to the StingRAY's power conversion system.

The following metrics will be estimated, and compared to the baseline StingRAY design, to evaluate the impact of the proposed solutions:

- Power Performance: percent improvement in annual mean electrical power at PWS
- Capital expense: capital cost of OVP, increase over the base system
- Reliability: mean time to failure (MTTF) for the improved OVP system

Annual mean electrical power (MEP) performance for the baseline and optimized designs will be evaluated using the PWS wave data. Efficiency reduction and/or power consumption due to OVP implementation will be accounted for. Periods of time where power production is offline due to OVP implementation will be accounted for. Net electrical power exported by the WPS will be utilized for the power performance metric.

The cost of OVP system components for the baseline and optimized designs will be estimated. The capital expense metric will be presented as a percent change with respect to the baseline design.

Mean time to failure (MTTF) for the OVP system will be estimated for the baseline and optimized designs based on their expected utilization (e.g., number of times triggered annually) using the modeled response in the OSS to represent an average year. The WPS will be assumed to be operating with 100% availability (aside from any OVP induced disconnects). The reliability metric will be presented as a percent change in mean time to failure with respect to the baseline design.

6.1.1 Detailed StingRAY Electrical Simulation Model

To assess the effectiveness of the proposed OVP methods, Cardinal Engineering created a detailed model of the StingRAY power system based on provided information and standard power system design practice. The model captures the overall StingRAY configuration and component parameters provided in the Power Plant Design description document [2] and controls as described in [3], a spreadsheet describing generator output characteristics into the AFE over a range of generator speeds for different damping ratios. A default damping ratio was used for the analysis. The generator, power converters, and other electrical components were modeled using standard Simulink components using parameters matching those of the StingRAY design. While reference [2] provides an overall description of the system operation and components, it did not provide enough information to develop detailed electrical models and control algorithms for all components. Where information was incomplete, Cardinal Engineering made assumptions based upon engineering judgement and industry standard design practices.

The top-level one-line diagram for the model is shown in Figure 9. The logic for the controls is in the System Control block, which is expanded in Figure 10.

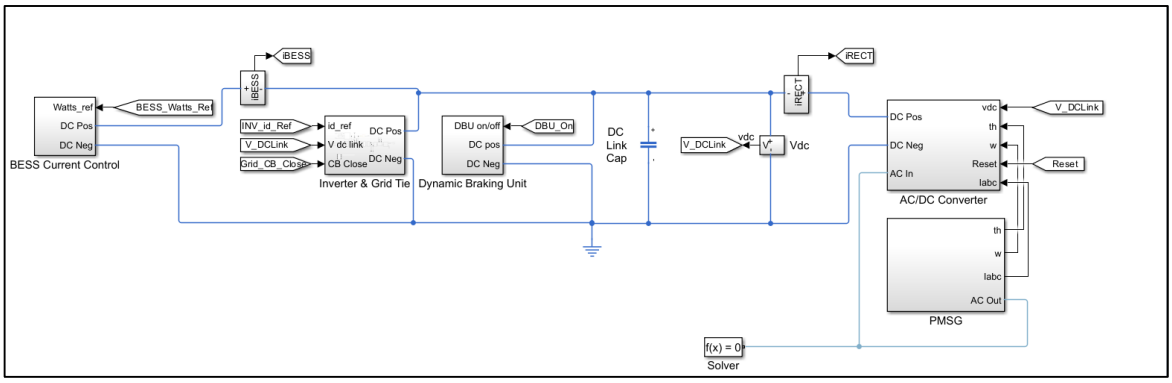

Figure 9. Top-level MATLAB Simulink model of the StingRAY power system.

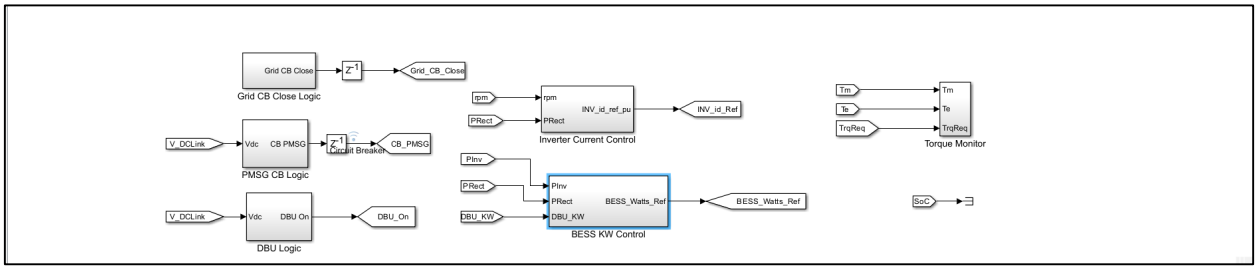

Figure 10. MATLAB Simulink StingRAY power system controls model.

Approaches for modeling each component were as follows:

- PMG: Cardinal Engineering drew upon a design report for the PMG “PM Generator Datasheet and Characteristic Curves” [3] and spreadsheet “CY20381-EfficiencyMapCalculation_JP2024_master.xlsm” [6] to derive generator characteristics. Because we didn’t have true open-circuit test or model results for the PMG operated as a standalone unit, we made assumptions on certain parameters and iterated the interaction between the PMG and AFE until characteristics matched those of [6]. The MATLAB Simulink implementation of the PMG, along with its mechanical speed input and output breaker, is shown in Figure 11.

The PMG was modeled using Simscape’s Permanent Magnet Synchronous Generator (PMSG) component as shown in Figure 11. The generator’s parameters such as the number of poles, flux linkage, and stator inductance were configured to fit the operating characteristics of the StingRAY PMG. The generator mechanical speed input is either an ideal sine wave velocity profile or one of the C-Power provided sea-state velocity profiles.

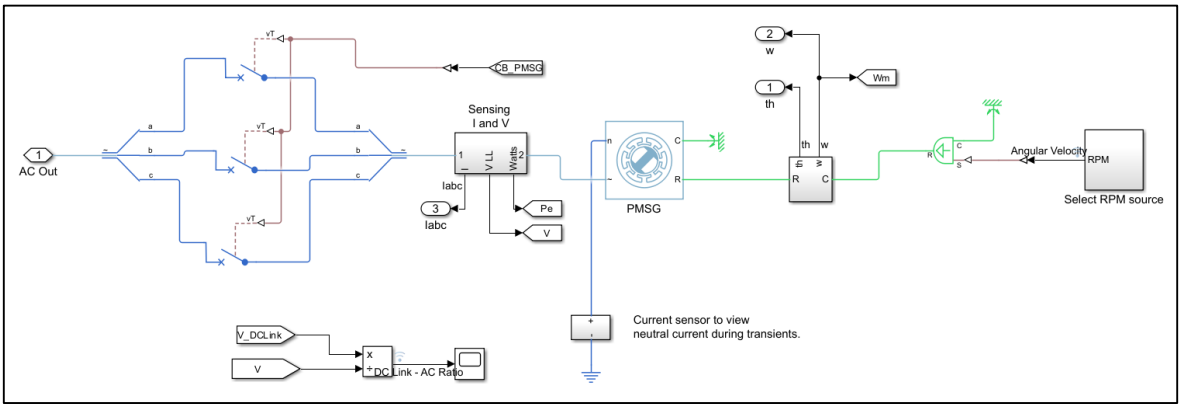

Figure 11. StingRAY Permanent Magnet Generator block subsystem.

- AFE: Figure 12 shows the AC/DC active front end converter model which models the low voltage drive hardware used for power conversion in the StingRAY system. The converter is modelled using Simscape's average-value voltage source converter (VSC) block which converts energy from the AC to the DC side based on a three-phase modulation wave. The average value voltage source captures the large signal behavior of the AFE but does not model individual transistor switches since that is of less interest for this study and would greatly increase model execution time. Controls are implemented to follow the different operating regions (constant torque, constant current, etc.) of the actual system. This is accomplished in the "Control" block.

AFE electrical characteristics are based on the information available in references [2], [6], [7], and standard motor drive practices. Options are implemented within the controls to enable optional d-axis current injection to reduce PMG terminal voltage. This is discussed in a subsequent section of this report.

The AFE rectifier is controlled in such a way that it draws power from the PMG consistent with the parameters given in [2] and [6] for the appropriate damping ratio. At low speed, the torque ramps linearly from 0 to the maximum allowable torque. In the medium speed range, the AC/DC converter draws a constant phase current equating to a constant torque equating to the maximum allowable torque. At high speed, the AC/DC converter draws current so that a constant mechanical power equal to the maximum power allowed is drawn from the PMG.

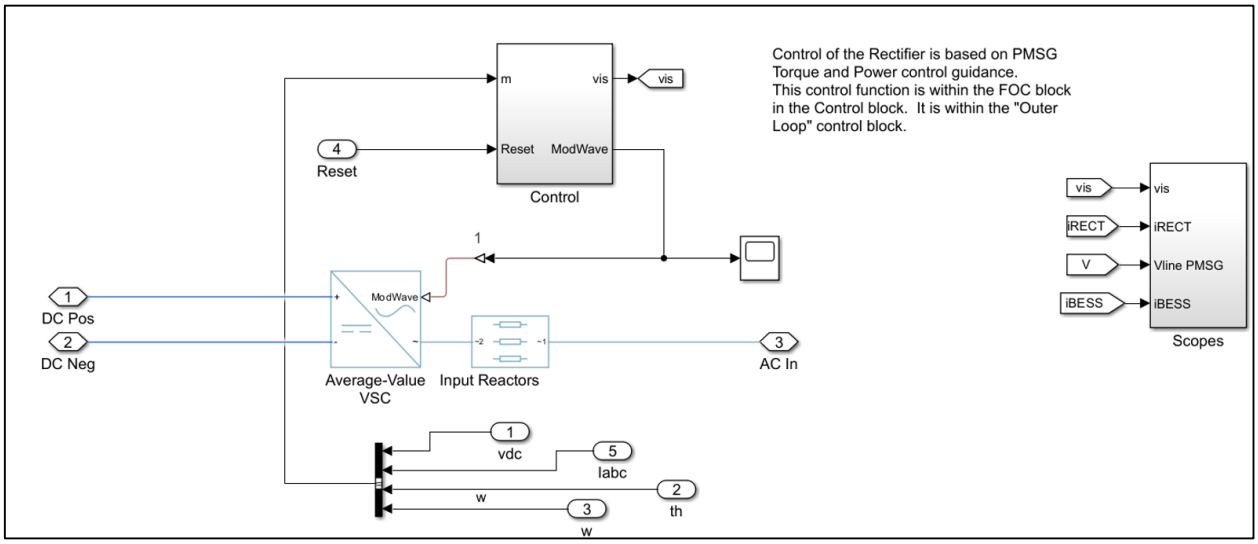

Figure 12. AFE AC/DC Converter subsystem.

• Dynamic Braking Chopper (DBC). The DBC is a chopper feeding a braking resistor. The model is based upon characteristics in [2] and [8]. The overall DBC system block diagram is shown in Figure 13 and the DBC control block diagram is shown in Figure 14. The exact control algorithm is not known so behavior is modeled to follow the general process of engaging the DBC at a DC link voltage of 1.042 PU and leaving it on until voltage returns to 1.0 PU (i.e. a 4.2% hysteresis). Note that the default controls limit the overall duty cycle to align with the maximum duty cycle allowed in the load resistor [8].

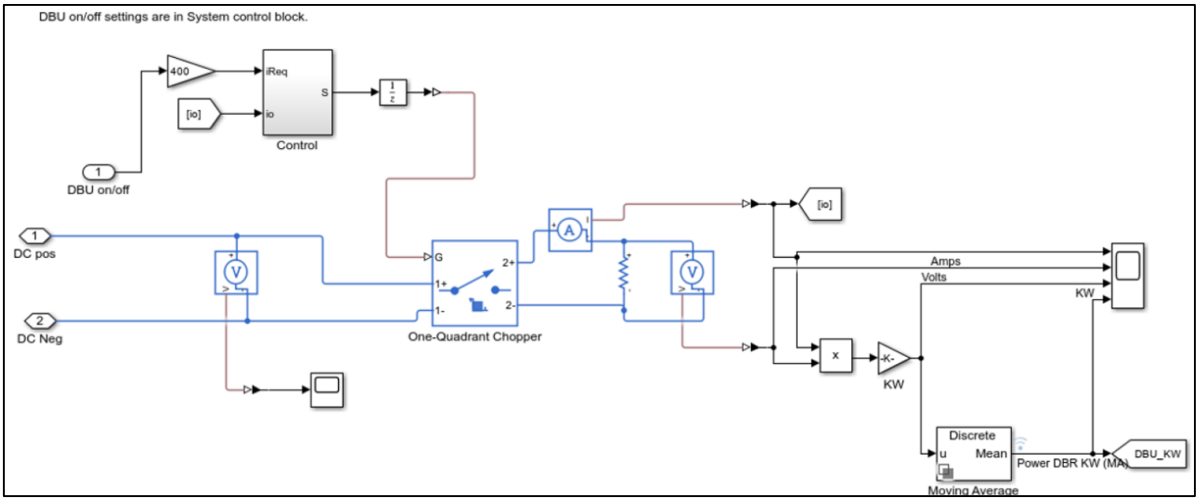

Figure 13. Dynamic Breaking Chopper (DBC) block diagram.

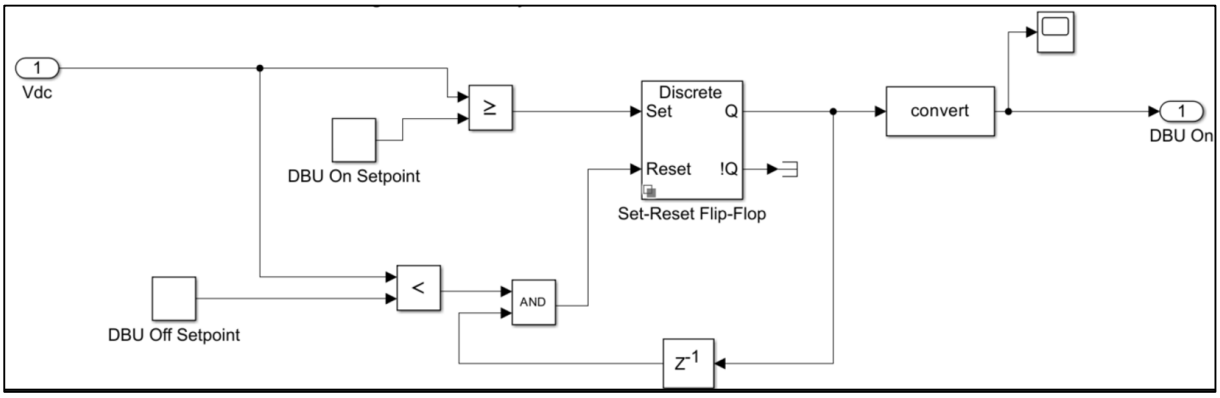

Figure 14. DBC control block diagram

• Battery Energy Storage System (BESS): The BESS consists of a DC-DC converter implemented via an AFE used as a three-phase interleaved buck-boost converter [2], DC inductors, a filter capacitor, and the battery module itself as shown in Figure 15. To model the battery accurately, Cardinal Engineering used discharge curves provided by the battery manufacturer. When power out of the AFE exceeds the power being output to the grid (which has a maximum limit based upon the transformer rating) to the grid, the BESS acts as an energy sink, absorbing excess energy. When generator output is low, the BESS acts as an energy source, supplying power to the grid. More sophisticated controls could be implemented in conjunction with the output inverter controls to maximize power delivery to the grid and further contribute to management of the DC link voltage by diverting energy into the battery during moments of pending over-voltage, but that was beyond the scope of this effort. The BESS is capable of absorbing much more energy than the DBC.

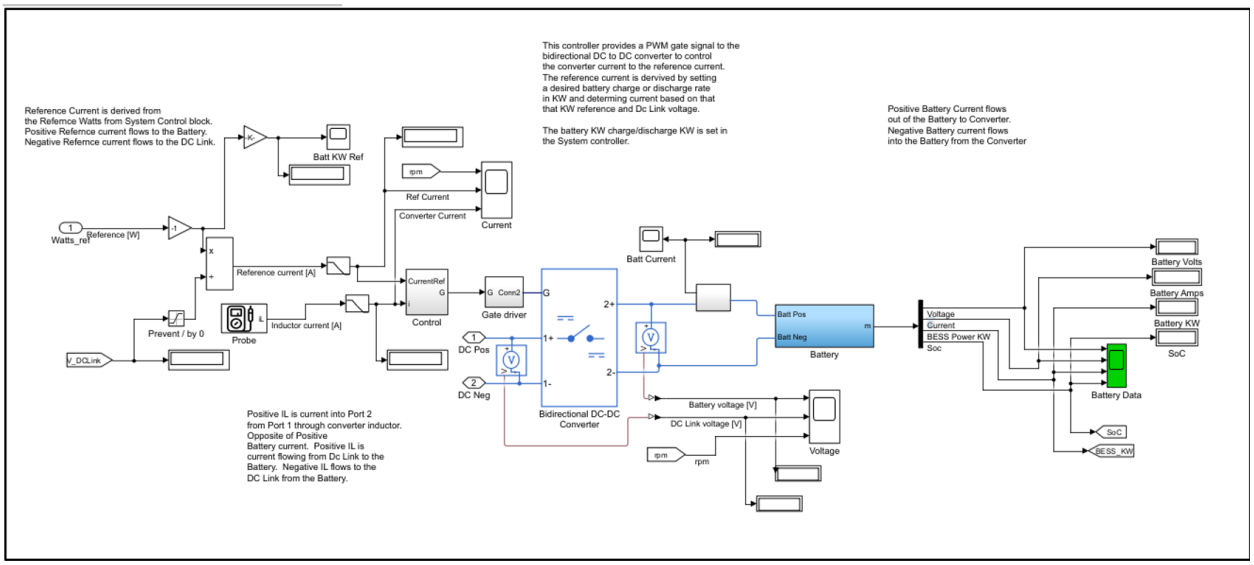

Figure 15. Battery Energy Storage System (BESS) block diagram.

- Grid Tie Inverter and Transformer: The model for the inverter, Figure 16, uses the average-value voltage source model of the AFE as an inverter to invert the system's DC link voltage to 60Hz AC voltage to be supplied to the grid through a low-voltage to medium-voltage transformer with characteristics per [2] and the transformer technical data sheet [9]. The controls are designed to pass the power generated by the PMG to the grid using a MATLAB Optimal Controller block fed by the output of the inverter control block, Figure 17. The basic controls follow the power output of the PMG but output a predefined minimum power and a maximum power that aligns with the kVA rating of the transformer. Controls could be optimized to draw upon energy storage to provide a smoother power draw during times of low generation at wave troughs but that was not within the scope of this project.

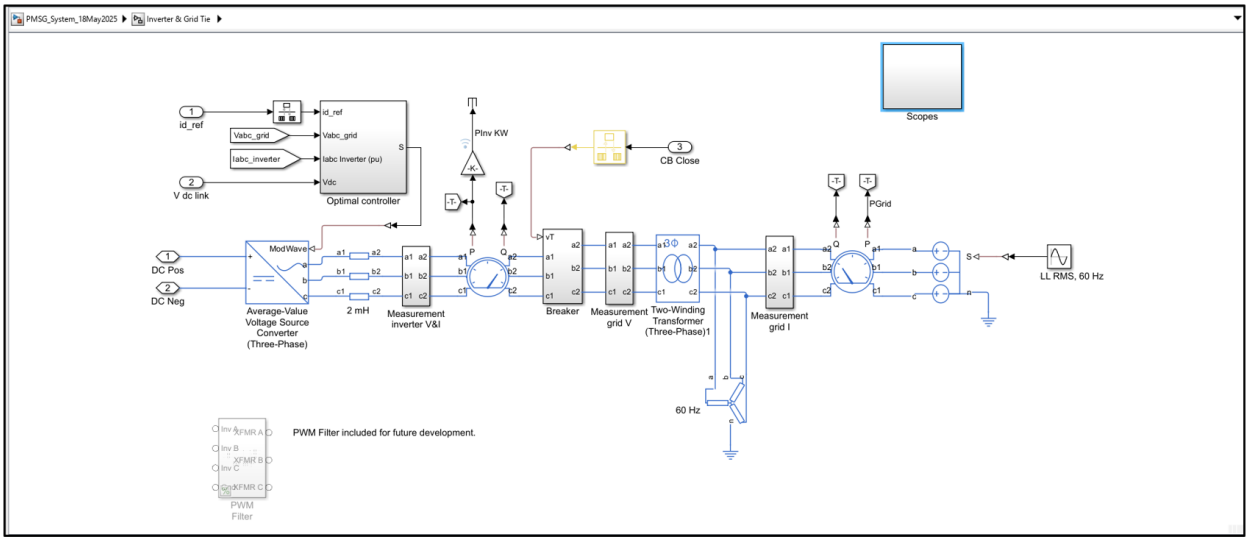

Figure 16. StingRAY model of Grid-Tie inverter and transformer.

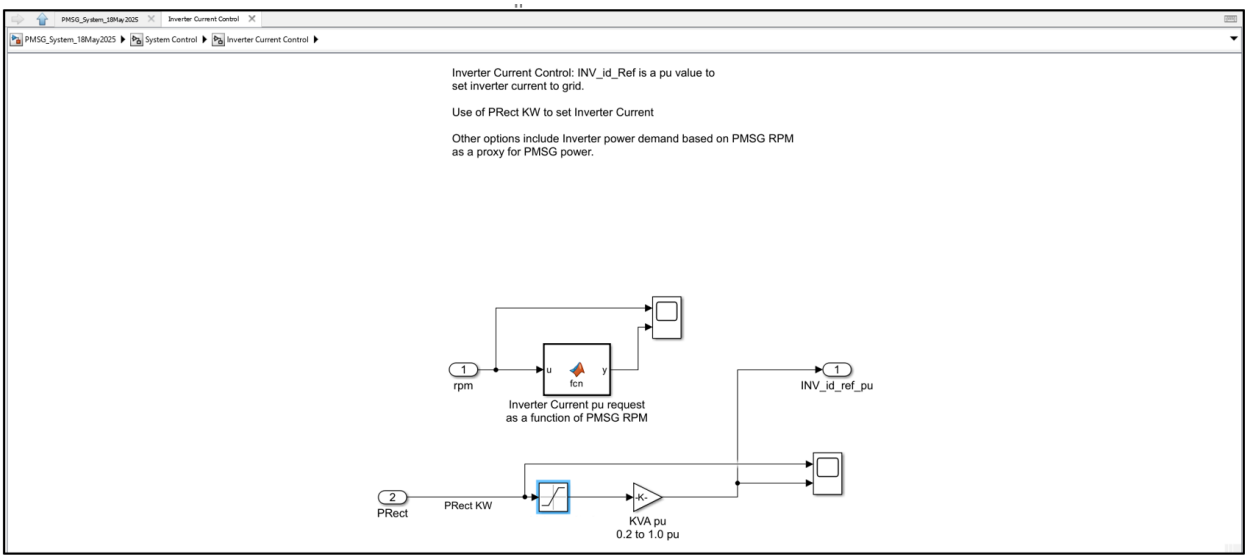

Figure 17. StingRAY model inverter control block.

6.2 Test and Analysis Matrix and Schedule

An analysis matrix identifying all tasks that will be performed and a corresponding schedule is presented in Table 3 and Figure 18, respectively.

Table 3. Analysis Matrix.

Task	Description
Requirements & Data Gathering	Establish parameter requirements for evaluation regarding the conditions of the over-voltage condition to include max voltage achieved, durations of over-voltage events, etc. and indicators of imminent over-voltage condition.
Preliminary Parameter Indicators	Generate the preliminary parameter matrix associated with the over-voltage event for analysis.
Preliminary Validation of Mitigation Methods	Build list of mitigation methods to be tested/evaluated based on the system indications. Run modeling of the expected outcomes of the mitigation efforts with respect to overall system net power output
Test Data Samples	Test run mitigation methods on simulation data
Design Optimization Analysis Iterations	Evaluate mitigation methods for net power out improvements based on larger data samples. Determine optimal mitigation method for StingRAY to improve the power generation overall output. Conduct scaled laboratory testing of OVP schemes.
Mitigation Method Cost Estimations	Determine changes in electrical system design and/or control concepts and costs due to new configuration
Final Design Model Updates	Revise model to reflect final mitigation design method
Post Access Report	Document findings with respect to design practices, performance impact, and cost impact
Post Access Questionnaire	Per TEAMER requirements

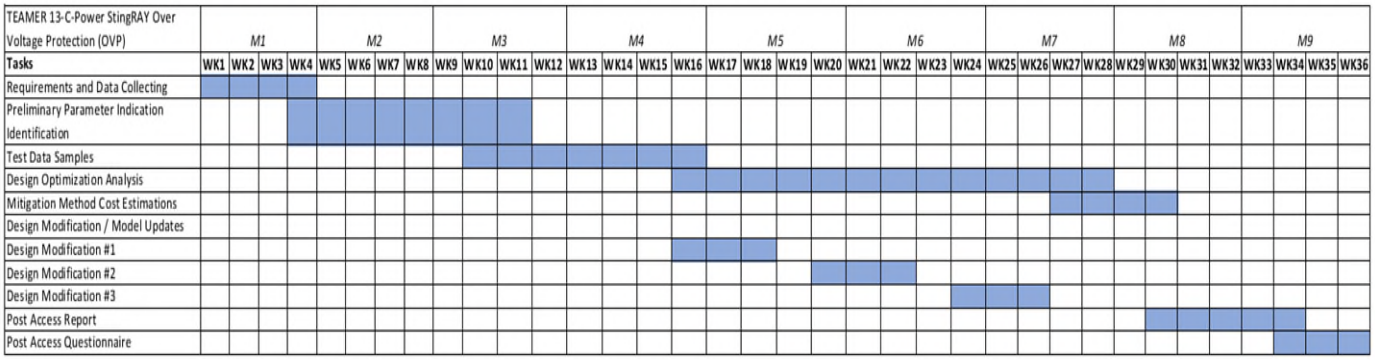

Figure 18. Project Timeline.

6.3 Safety

This is a numerical simulation with low voltage controller testing in a lab environment; Cardinal has an established safety process for laboratory work. No additional safety procedures and protocols are needed.

6.4 Contingency Plans

No project contingency plans are anticipated currently.

6.5 Data Management, Processing, and Analysis

6.5.2 Data Management

C-Power will supply Cardinal Engineering with baseline design information of the StingRAY.

Data provided to Cardinal Engineering from C-Power may be in the following formats:

- MATLAB (.mat) or (.m) files
- Comma Separated Value (.csv)
- Microsoft Excel Spreadsheet (.xlsx or .xls)

During and at the conclusion of the analysis and design processes, Cardinal Engineering will supply C-Power with all resulting data in native formats. Associated data will be in the forms listed below:

- Electrical system mitigation method time history – MATLAB tables (.MAT)
- Electrical diagrams and OVP specifications as applicable
- Supporting hand calculations (as applicable) – Excel spreadsheets
- Cost data – information gathered to support cost assessments will be summarized in the final report

It is planned for C-Power to evaluate the mean annual power performance for their baseline and final selected mitigation method (design change) to examine the impact of changes/improved system net power output versus baseline.

Cardinal Engineering will store and safeguard all data and work products within our internal corporate IT infrastructure.

In addition to the narrative final report detailing findings, C-Power and Cardinal Engineering anticipate uploading the following data to the MHKDR: MATLAB (.mat) or (.m) files, Comma Separated Value (.csv) and Microsoft Excel Spreadsheet (.xlsx or .xls) files. While C-Power may reserve certain StingRAY-specific design details that are commercially sensitive, design practices developed through this study and their impacts on the StingRAY case study will be thoroughly documented and made available for public distribution through the post-access report and technical conference.

6.5.3 Data Processing

Identifying and implementing sound data processing methodologies are a key component of project success. The C-Power supplied simulation data serves as the basis for the regressive data analysis in MATLAB by Cardinal Engineering. This data was sorted for over-voltage events, and key pre-event variables will be extracted to form the basis for the regressive data analysis. A data processing algorithm that targets magnitude and duration of over-voltage events and the associated power output gains from the proposed solutions will be developed and integrated. The data set supplied by C-Power features thousands of events, so anomalies in the data could be identified and outliers can be excluded from the analysis and system design. These outliers would be more appropriately addressed with emergency protection devices versus the normally operating suppression equipment.

If predictive data trends are discovered, the algorithm would also examine data during normal operation to ensure that false positives do not unnecessarily trigger the implementation of the solution. This can help ensure reliability of the system and eliminate uncertainty from the results.

The CHIL test bed used standard data acquisition equipment with calibrated sensors. These sensors are routinely used in industry and are considered accurate and reliable. The data reliability of the test bed has not been identified as a high-risk item. If the solution were to be implemented in the field, a more complete design of a ruggedized, high power, high-rate system would occur at that time.

6.5.4 Data Analysis

MATLAB was used to produce plots that demonstrate performance of the proposed solutions. These included pre and post solution voltage versus time plot for specific events and annual net power output calculations.

7. Project Outcomes

7.1 Results

Cardinal Engineering's work in support of the C-Power StingRAY OVP project consisted of two main efforts:

1. Modeling and simulation to evaluate different methods of OVP.
2. Testing and evaluation of a solid-state switch to disconnect the PMG from the AFE rectifier upon detection of a condition that could cause a DC link over-voltage.

The information gained from these two efforts informed the selection of the preferred methods of OVP. The baseline for comparison was the original powerplant design document which provided a trip threshold of 7.61 RPM using a conservative DC link trip threshold of 1.08 PU. Using the system model and factoring in voltage drops across system impedances and the voltage regulating effects of the DBC, BESS, and energy output to the grid, simulations showed that the trip threshold could be raised to 8.5 RPM. This uses a less conservative trip threshold of 1.135 PU, accounting for the fact that the disconnect switch will be a fast-acting disconnect switch that rapidly removes power upon activation

7.1.1 Modelling and Simulation to Evaluate Different Methods of OVP

Once the model described in section 6.1.1 was functional, Cardinal Engineering analyzed the effects of standard operation of the BESS and DBC on the DC link voltage to see how their operation helps mitigate over-voltages. We also explored design changes that could potentially mitigate over-voltage. Options considered were:

- Addition of load on the AC side of the generator to pull voltage down. This was deemed non-viable due to the large size of the load bank that would be required.

- Insertion of a series impedance between the PMG and AFE during times of impending over-voltage. This was deemed non-viable for the same reason. The size of load that would be required to reduce voltage would have been in the hundreds of kW.

- Refinement of BESS and inverter controls to regulate DC link voltage. In the same way that the DBC works by applying real power load (as opposed to reactive power) to regulate the DC link by diverting energy from the DC link capacitors, we explored whether we could similarly load the DC link by tailoring the power flow into the BESS by the DC-to-DC converter or the power flow pushed out onto the grid by the inverter. We did some exploration of this concept but fully implementing it would have required substantial changes to the overall notional control system operation. We were not certain whether these changes could have been implemented within the power electronics drive architecture and did not finalize the concept.

- Use of a solid-state or other fast-acting switch to disconnect the PMG from the rectifier during times of impeding over-voltage and rapidly reconnect it when the wave has subsided. This concept is deemed viable and was explored in a sub-scale hardware test described elsewhere in this report. During the late stages of data analysis, we found that the solid-state switch contributed significant loss to the system and assessed alternative mechanical switches that could sustain a high number of operations while switching quickly enough to avoid excessive downtime.

- Use of a concept called flux weakening or field weakening. Flux weakening is achieved by drawing a level of direct axis current (id) from the PMG into the AFE rectifier. Current drawn at this angle creates opposite flux to that produced by the permanent magnet rotor and hence reduces the PMG output voltage. This is intended to enable operation at higher speeds while maintaining an acceptable output voltage at the input of the AFE rectifier which, in turn, lowers the DC link voltage.

    - Flux weakening was implemented within the control block of the AFE AC/DC converter (Figure 12). Within the control block, all controls are contained with a field-oriented control (FOC) subsystem (Figure 19). The outer loop block of the FOC subsystem (Figure 20) provides reference quadrature axis current (i_q) and direct axis current (i_d) commands to the Current Control subsystem, which in turn, provides the signal as an input to MATLAB's PMSM Current Controller with Pre-Control standard block.

    - At generator velocity below 7.35 RPM, the i_d command to the Current Control is set to zero. When flux weakening within the model is implemented, a negative i_d command is calculated per the Qref to id_Ref block, the logic of which is shown in Figure 21. When generator velocity rises above 7.35 RPM, d-axis current is injected to oppose the inherent magnetic field within the PMG. The

maximum injected d-axis current is limited to ensure total system current does not exceed the maximum allowable current.

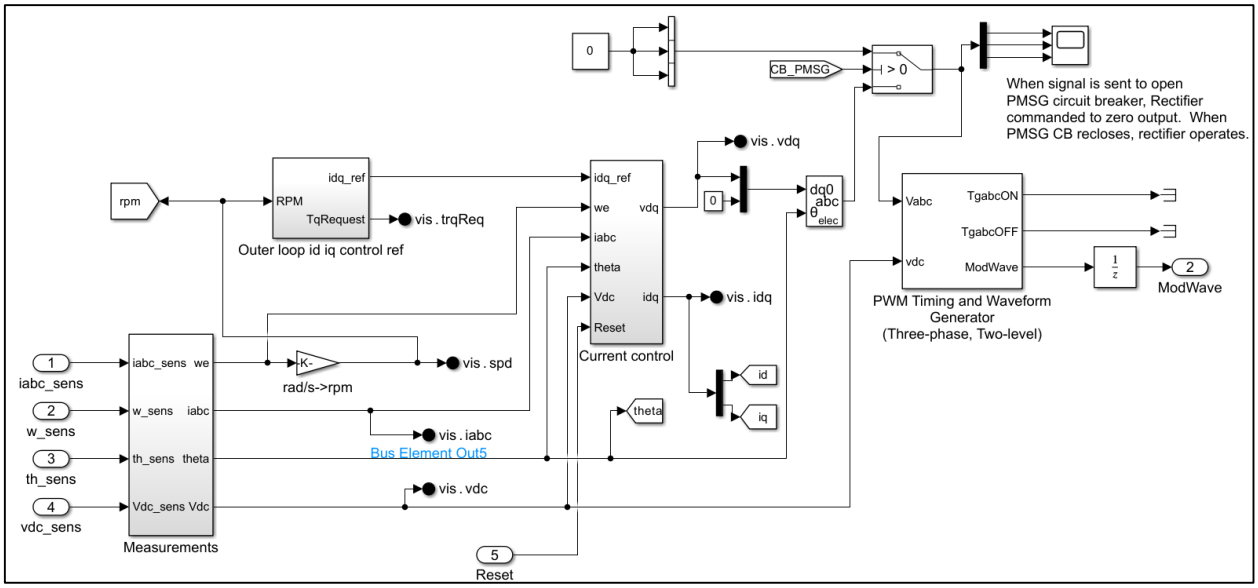

Figure 19. Field oriented control block of the AC/DC converter.

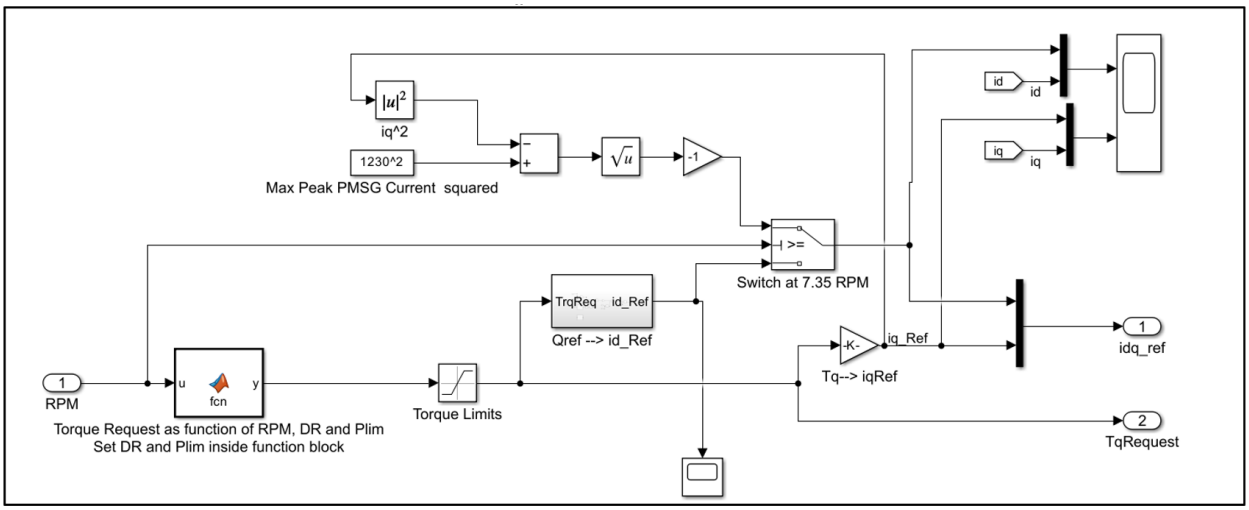

Figure 20. Flux weakening control for StingRAY implemented in the Outer loop i_d i_q control ref.

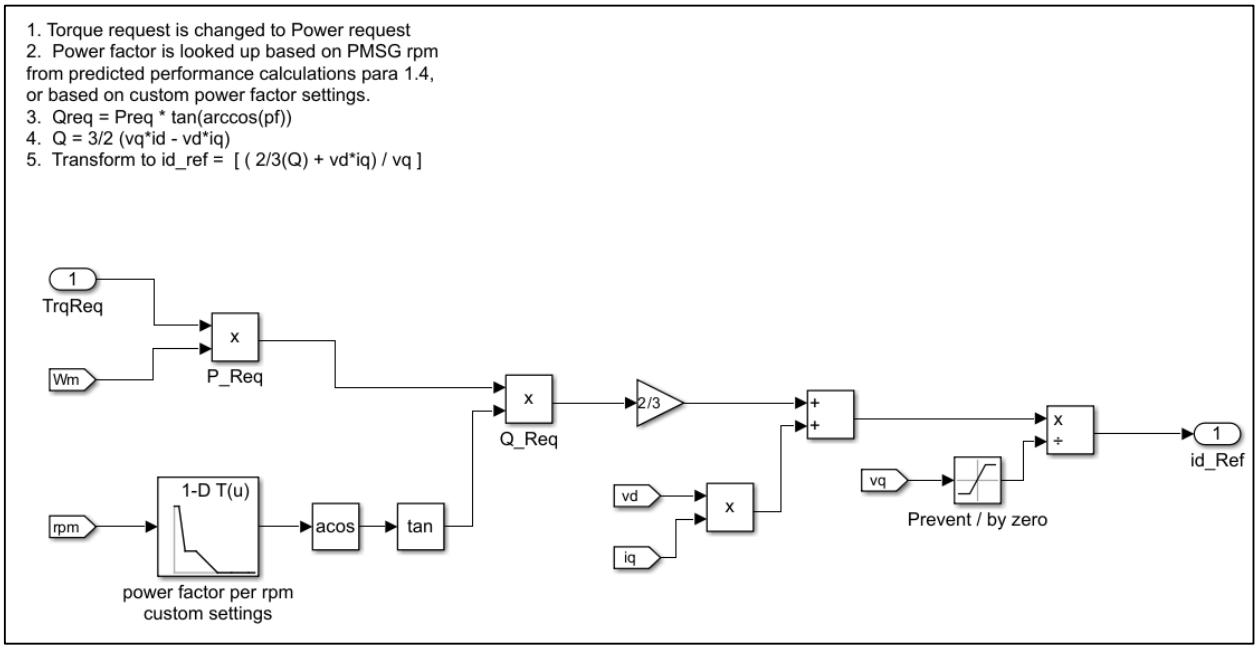

Figure 21. Qref to Id_Ref block for implementation of flux weakening.

To determine the effects of the BESS, DBC, and flux weakening; simulations were run with and without the components enabled. To simplify simulation and provide a common reference, two series of simulations were run using a 10.1 and 12 peak RPM amplitude sine wave, each with a period of 4 seconds (Figure 22).

Results for a peak speed of 10.1 RPM showed that operation of the BESS and DBC contribute substantially to regulation of the DC link voltage. If both are enabled and operating in accordance with the controls described above, the maximum RPM goes increases around 7.61 RPM to 8.47 RPM (red line in Figure 22) without an overvoltage trip. Addition of flux weakening further raised the maximum RPM without a DC link over-voltage trip to 10.1 RPM (blue line in Figure 22).

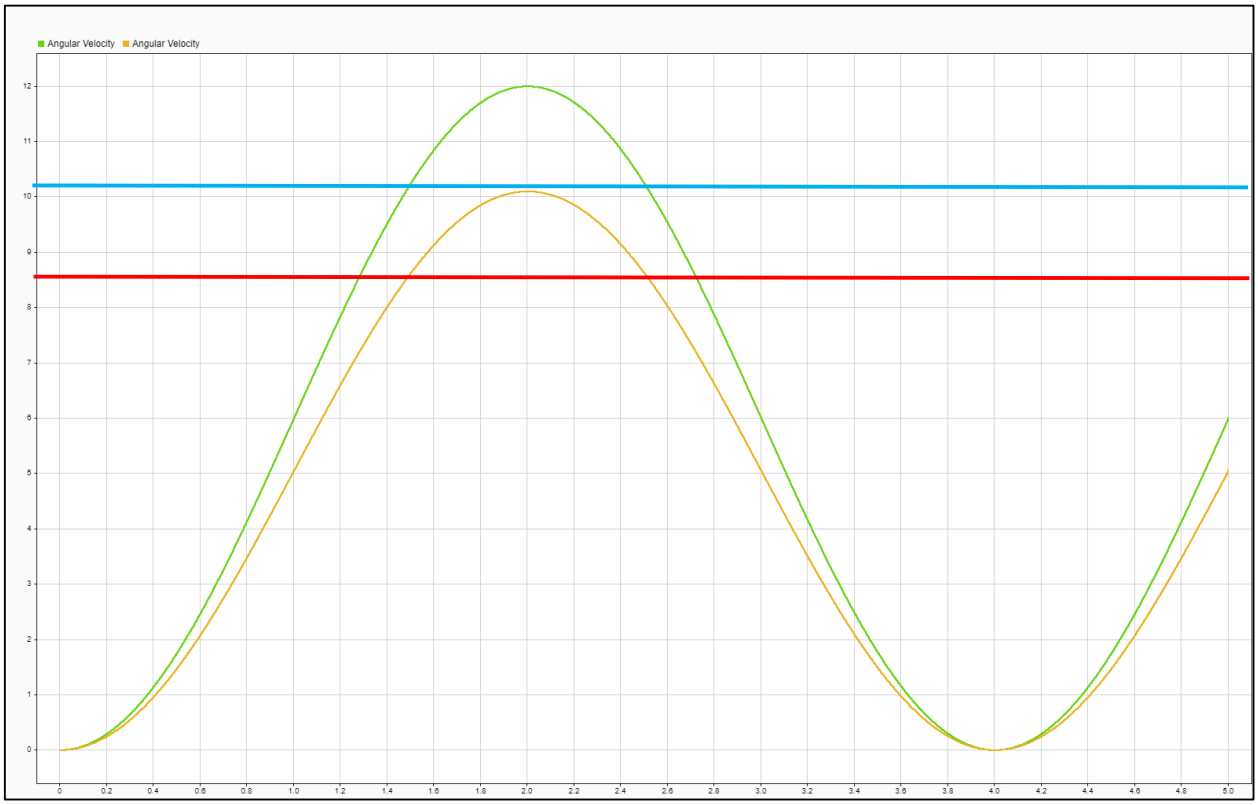

Figure 22. Plot of 10.1 (yellow) and 12 (green) peak RPM velocity profile used to characterize over-voltage protection mitigation strategies.

A plot showing the effects of flux weakening on simulated PMG output voltage is shown in Figure 23. The blue trace shows the voltage without flux weakening and the maroon trace shows the voltage with flux weakening. In this instance, flux weakening delayed the over-voltage trip by 0.2 seconds for this particularly high RPM wave. In many instances, raising the trip level from 8.5 to 10 RPM avoids tripping altogether, reducing annual OVP events and increasing availability.

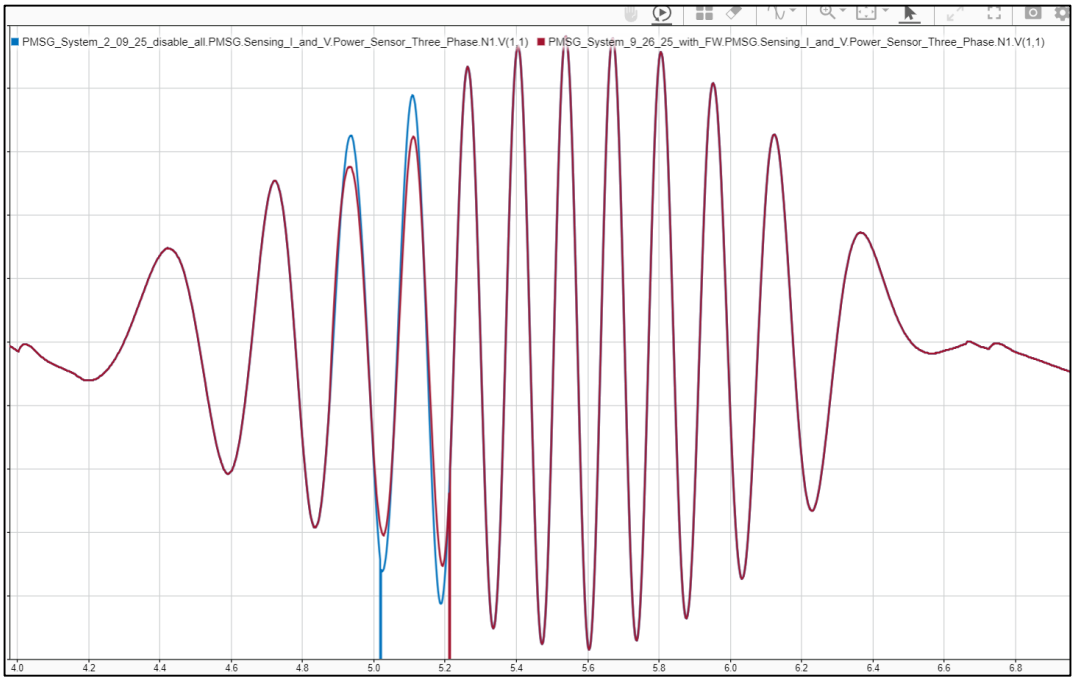

Figure 23. Reduction in PMG voltage due to flux weakening. Flux weakening in effect from 4.9-5.2 seconds, reducing peak voltage by >10%.

To ensure that flux weakening would work for a representative RPM profile and not just the sine wave profile shown in Figure 22, the model was run using data from the worst-case speed profile from [1] with the BESS and DBC operational with and without flux weakening. The plot of rotor speed, DC link voltage, PMG phase B current and PMG phase A voltage over a 12-second period with the highest speed is shown in Figure 24. A magnified view of this same data is shown in Figure 25. The point at which the PMG is disconnected can be determined by the time at which the current in the bottom left-hand plot stops flowing. Following are a few observations about this data:

- The case without flux weakening trips at a speed of 8.5 RPM, consistent with the above analysis.
- The case with flux weakening trips at a speed of 9.9 RPM, consistent with the above analysis.
- The current plot, bottom left, shows how injection of d-axis current increases the phase current to the maximum allowable level when flux weakening kicks in at 7.35 RPM.
- The decrease in phase voltage due to flux weakening can be clearly seen in the bottom right plot. Curser measurements show that the peak phase voltage decreases by 0.11PU.
- The negative-going spike in the bottom right plot is an $L\frac{di}{dt}$ voltage spike that occurs due to the way the switching device is modeled. The switch model instantaneously chops current whereas a thyristor-based switch would commutate off more gently.
- The real value in flux weakening would not be for cases like shown below. Flux weakening only allows approximately 0.2 seconds additional operation compared to the case without flux weakening. The true value of flux weakening comes from allowing the system to continue to operate during those cases with a peak speed between 8.5 and 10 RPM where the flux

weakening prevents, rather than delays, a trip that would normally occur without flux weakening, increasing the annual up time.

- We assessed whether the increased current due to flux weakening would cause additional losses that would counteract the increased efficiency due to the reduced downtime. We determined that it did not. Flux weakening only kicks in when speed exceeds 7.35 RPM. Per [3], 7.35 RPM equates to 0.94 PU voltage. This voltage level is reached only a small percentage of the time, so the increased current occurs so infrequently that it would not contribute significantly to loss. For example, Figure 26 shows a snapshot of output voltage from MATLAB data in N7638cs81.mat from [1], which is one of the worst-case speed profiles. The orange line shows the voltage threshold at which flux weakening is initiated. It is clear that this is a tiny fraction of the overall operating time.

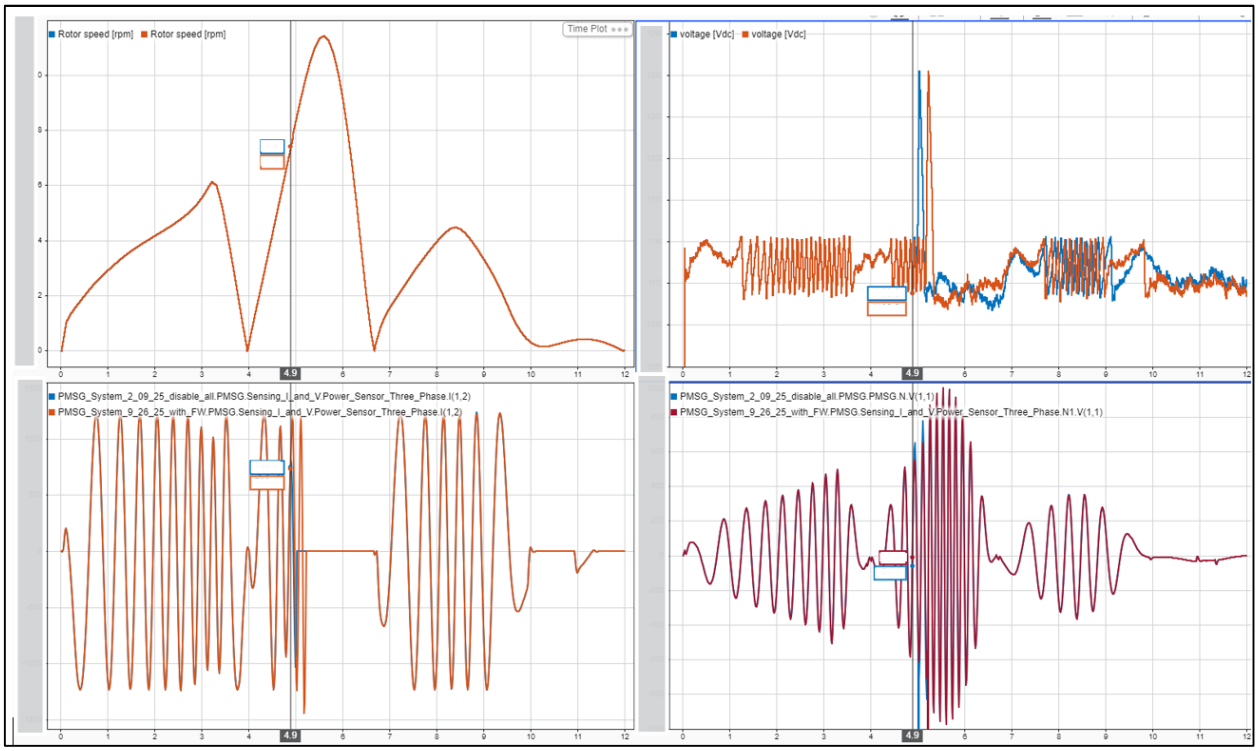

Figure 24. Simulation data with C-Power-provided generator speed input. Blue traces are without flux weakening. Maroon traces are with flux weakening. Top left: PMG RPM, Top right: DC link voltage, Bottom left: PMG phase B current, Bottom right: PMG phase A voltage.

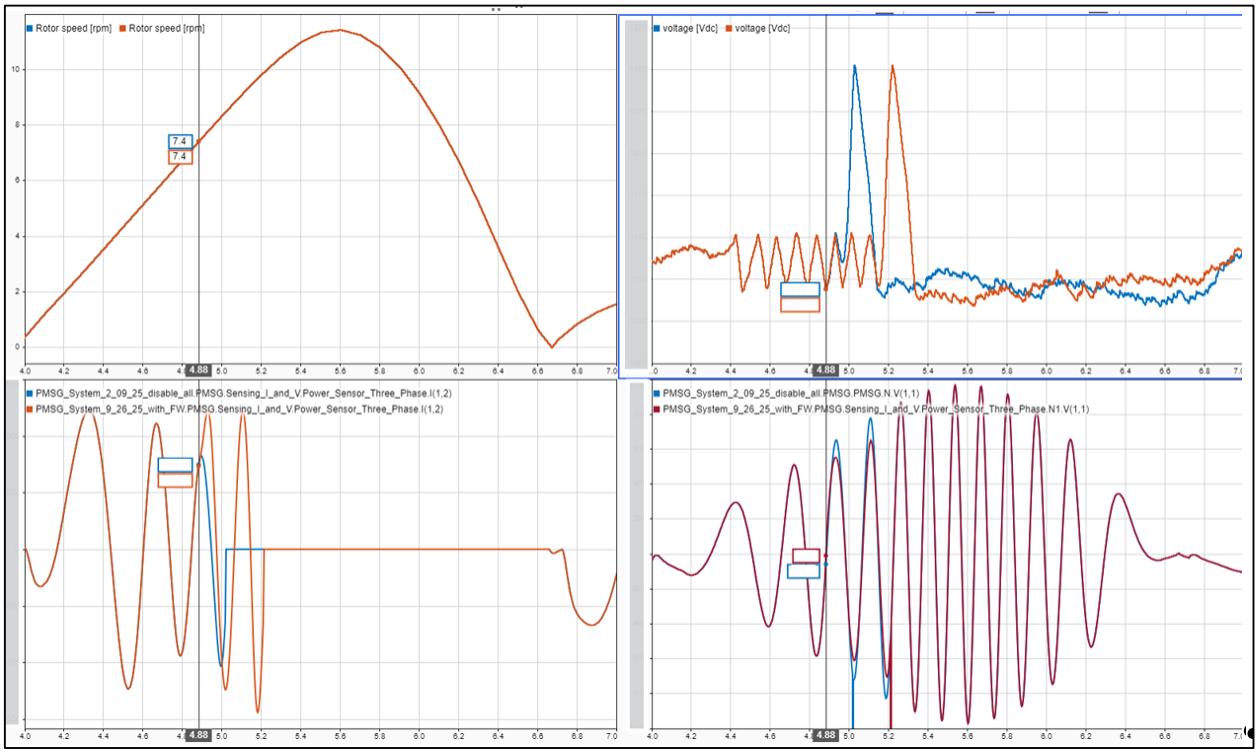

Figure 25. Zoom of simulation data with C-Power-provided generator speed input. Blue traces are without flux weakening. Maroon traces are with flux weakening. Top left: PMG RPM, Top right: DC link voltage, Bottom left: PMG phase B current, Bottom right: PMG phase A voltage.

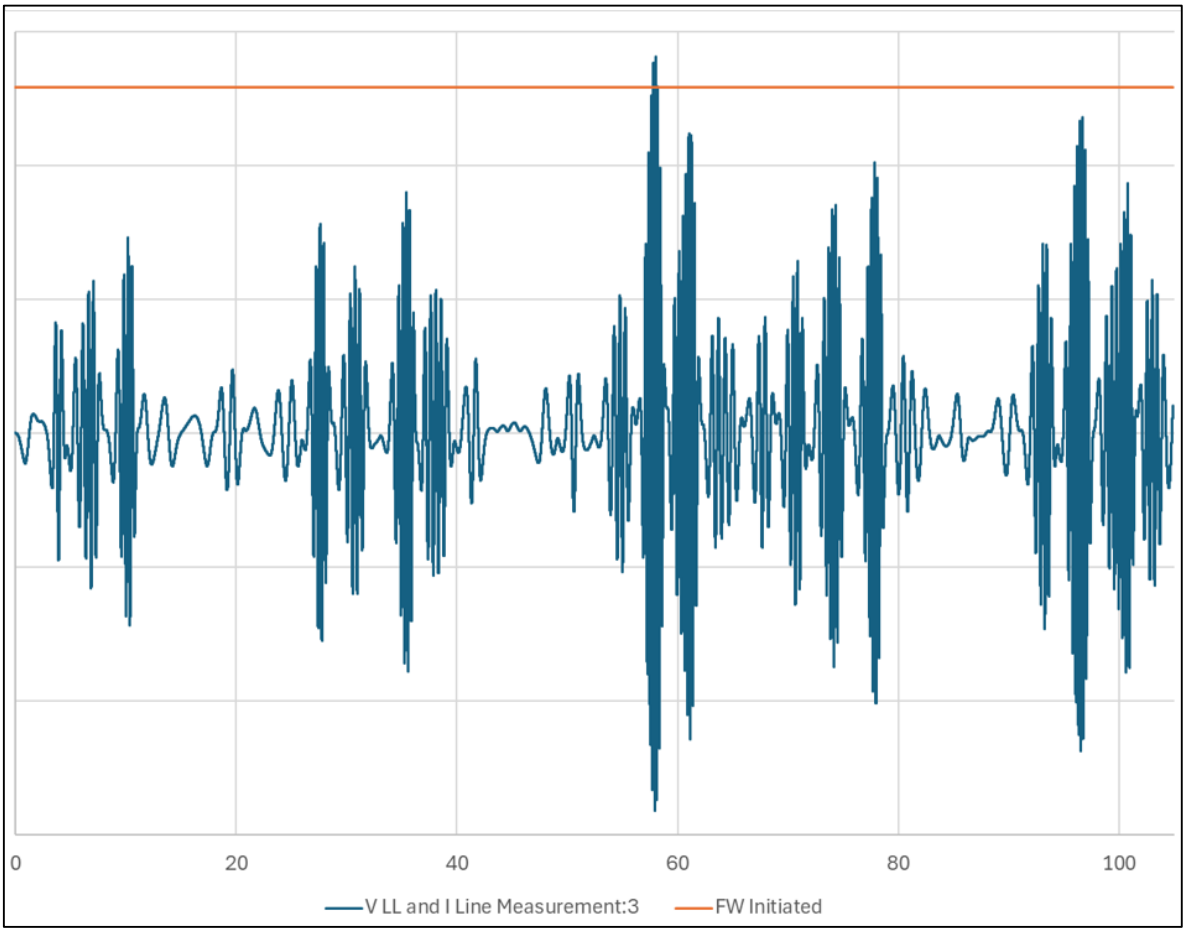

Figure 26. Snapshot of output voltage from MATLAB data from the worst-case wave conditions. Orange line shows when flux weakening is initiated.

The BESS power (negative indicates BESS charging, positive indicates BESS discharging), PMG power through the rectifier, inverter power to the grid, and DBU power are shown in Figure 27. Following the load profile provided in [2], the BESS charge rate was limited to 64% of its full rating listed in [2] and the BESS discharge rate was limited to 13% of the full rating. Allowing stronger charge rates during high DC link conditions could help mitigate the voltage rise.

Similarly, the inverter output power is limited due to the transformer rating. If this limit is raised momentarily during pending over-voltages, this could help mitigate the voltage rise. The minimum output power was selected to be 18% of the transformer rating based on assessment of the wave data in the speed profile used. This variable would need to be adaptable to the wave profile so as not to deplete the battery state of charge or allow the battery to overcharge.

The DBC power is shown in the bottom right. Note that the DBC duty cycle limitation results in a lower power than the full power rating would allow if unrestricted.

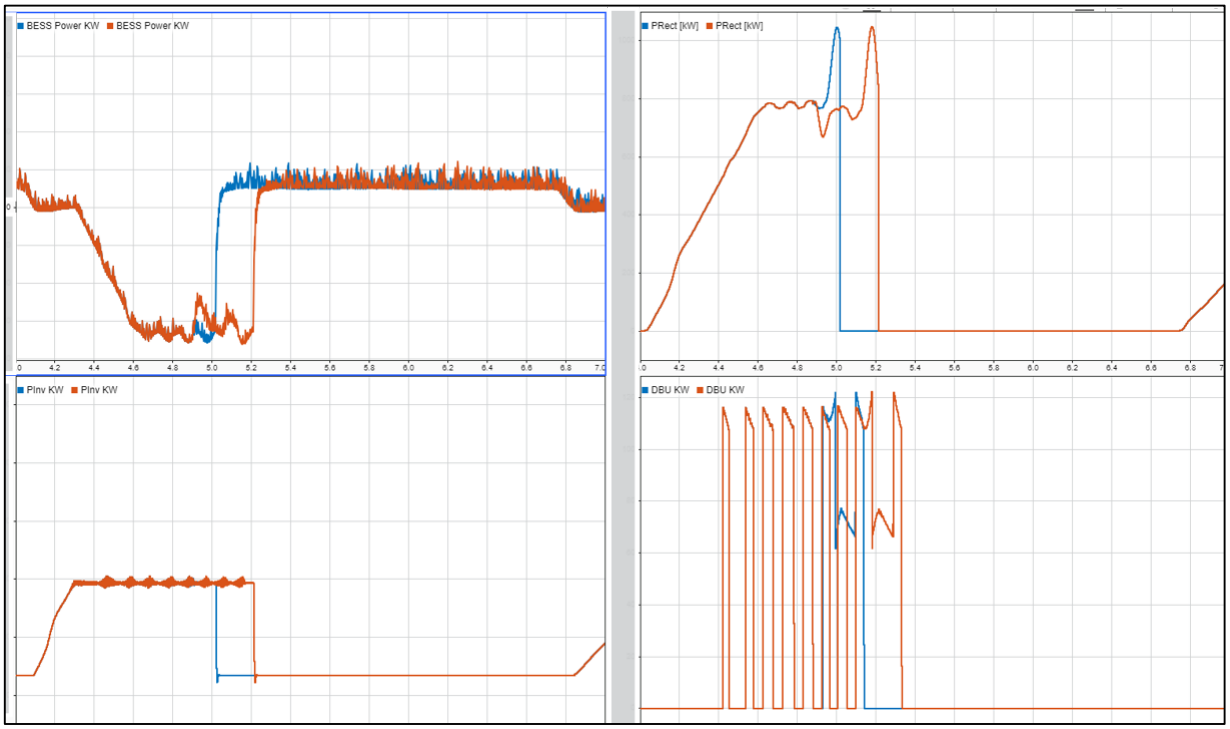

Figure 27. Simulation data with C-Power-provided generator speed input. Blue traces are without flux weakening. Maroon traces are with flux weakening. Top left: BESS power, Top Right: PMG power through the rectifier, Bottom left: inverter power to the grid, Bottom right: DBC power

As with the sine wave data, this data shows the effectiveness of flux weakening in raising the maximum sustainable RPM without DC link over-voltage from 8.5 to 9.9 RPM. While this isn't sufficient to eliminate all expected trips that could be expected, it is a worthwhile increase that will increase the efficiency of the StingRAY system.

7.1.2 Testing and evaluation of a solid-state switch to disconnect the PMG from the AFE Rectifier upon detection of a condition that could cause a DC link over-voltage.

The purpose of this lab demonstration is to provide a proof-of-concept for one of the direct over-voltage protection (OVP) methods for the StingRAY wave energy generation system. The function of this proof-of-concept OVP system is to monitor the voltage at the output of an emulated PMG and disconnect it from the AFE rectifier upon detection of conditions that could lead to a DC link over-voltage. As discussed above, mechanical contactors are not suitable as disconnect devices because of their limited number of operating cycles and slow response time. Insulated-Gate Bipolar Transistors (IGBTs) are also unacceptable as input switching devices because their relatively high on-state voltage would result in losses that would require an active cooling system. Also, because IGBTs chop the current to zero immediately upon switching, the system would experience a high voltage transient due to the sharp $\frac{di}{dt}$ during turn-off due to the PMG's internal inductance and the AFE rectifier's input reactors (recall that voltage across an inductor is $L \cdot \frac{di}{dt}$). We chose silicon-controller rectifiers (SCRs), also known as thyristors, as our switching devices because of the following characteristics:

- They have a relatively low on-state voltage, hence relatively low losses, compared to other semiconductor switches.
- Their hockey-puck construction gives them high thermal mass and two cooling surfaces, allowing them to tolerate momentary over-currents better than module-based devices. In other words, they have a larger safe operating area (SOA) compared to other semiconductor devices.
- Upon removal of their gate signal, they behave like a diode until the next current zero crossing at which point they commutate off. This results in a "gentler" turn off with lower voltage transients.

With the type of switching device selected, Cardinal Engineering designed and built a lab-scale SCR-based OVP device that senses AC voltage and removes the gate drive from the SCRs upon detection of conditions that could cause an over-voltage (Figure 28). For the SCRs, two Hitachi 5STP 16F2810 High Power Thyristors were used, configured in an anti-parallel configuration. These are sized for use in the real system, rated for up to 2800VRMS and 2360ARMS. The voltage sensor used was the LEM DVL 150 Hall Effect voltage sensor. The DVR 150 is capable of sensing voltages up to ±225V, although they have models capable of sensing up to ±3000V. Given the low frequency nature of the system, we opted for a sensor designed to sense instantaneous voltage rather than one that derives RMS voltage. The DVL 150 converts the sensed voltage into a current signal between ±75 mA. For the Microprocessor Control Unit (MCU), we used an STM32H747XI which is a dual core 32-bit MCU populated on a development board (Arduino Giga R1 Wi-Fi). Custom peripheral voltage processing circuitry was designed to convert the output current signal of the DVL 150 to a 0-3.3V signal that the MCU could read along with a circuit to control the gate drivers of the SCRs. For the gate drivers, we used APS's BAP-1106 SCR Gate Drivers.

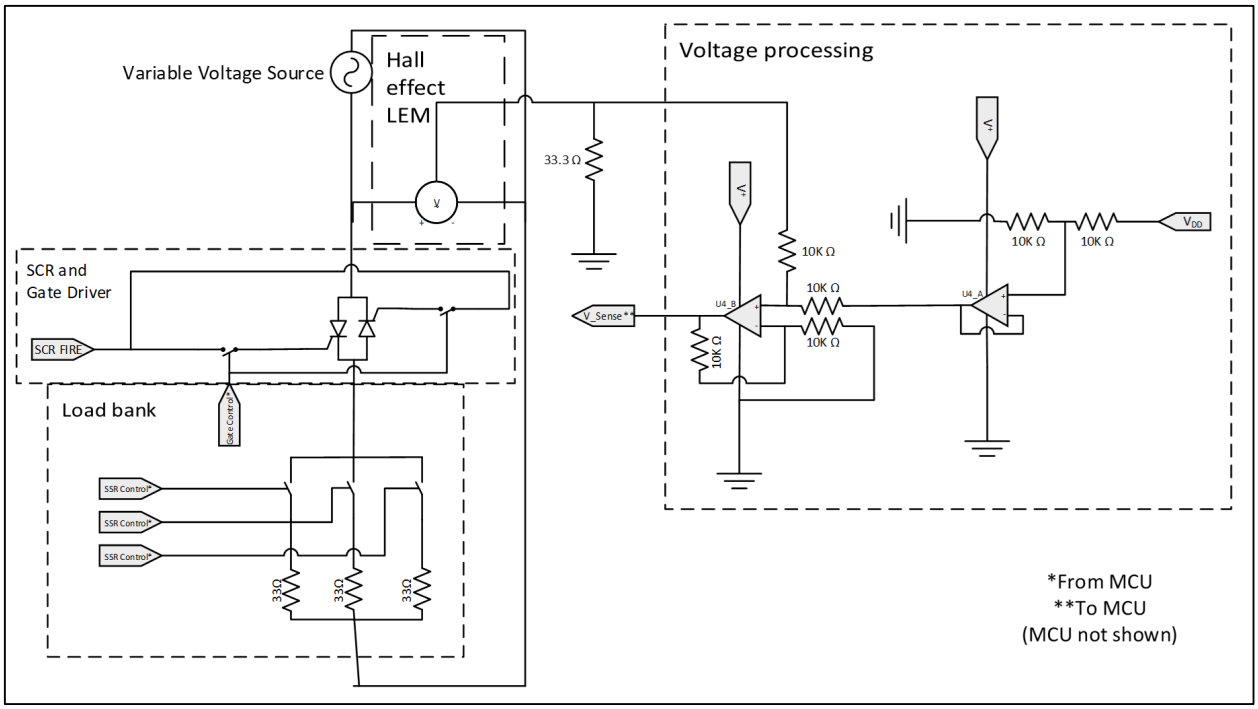

Figure 28. Lab-scale single-phase OVP device. Power supply and load bank also shown.

Cardinal Engineering also designed and built a test bed to evaluate the OVP system. The test bed consisted of a Pacific Power 6kVA 360AFX-2AG AC+DC power source, a fixed resistive load bank, interconnecting cabling, data acquisition equipment, and a computer to program the power source. For the load, fixed resistors, were used. An oscilloscope was used to measure the voltages at various points in the circuit.

An overview of the test bed is shown in Figure 29. Pictures of the lab-scale OVR and test bed are shown in Figure 30 and Figure 31, respectively.

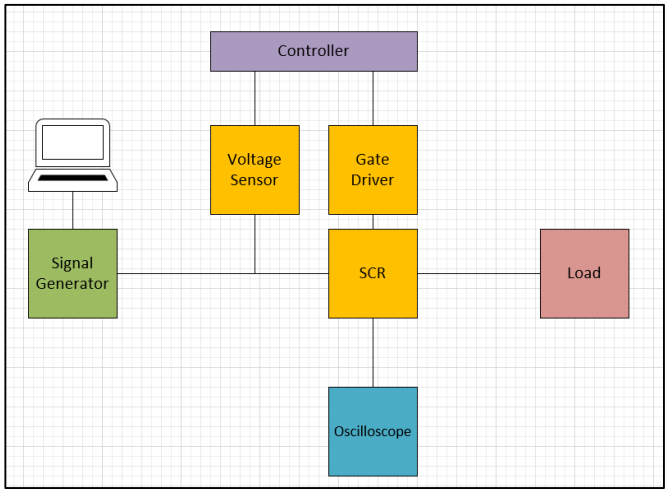

Figure 29. OVP test bed overview.

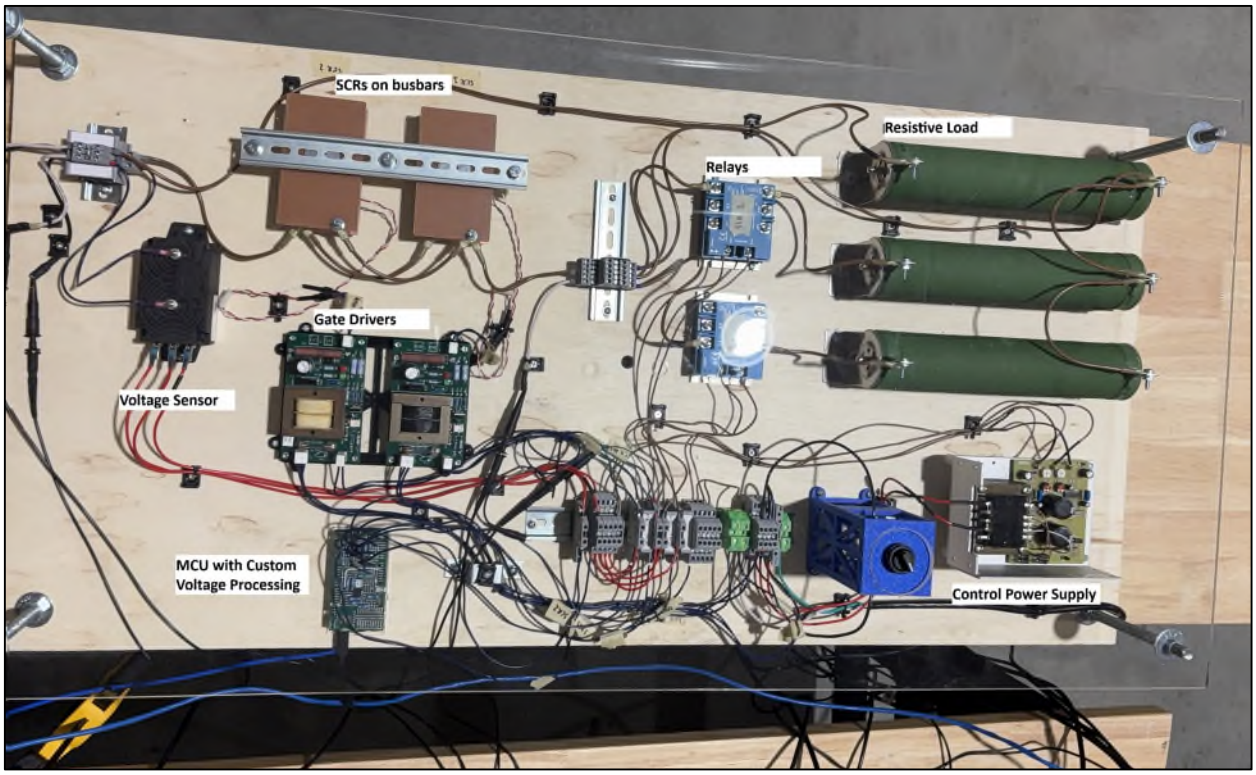

Figure 30. Top View of Lab-Scale OVP and Resistive Load.

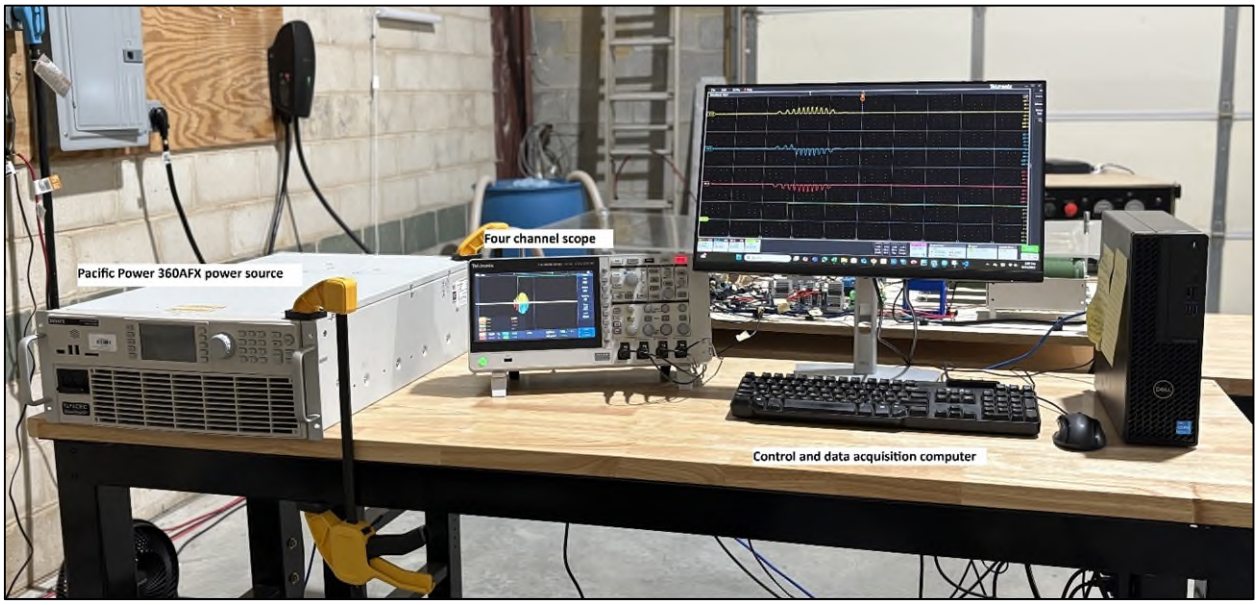

Figure 31. Test bed power supply and control/data acquisition equipment.

A top view of the entire test setup with cooling fan and plastic safety cover over the energized components is shown in Figure 32. To enable portability and storage for future work, the components were mounted on a wooden board.

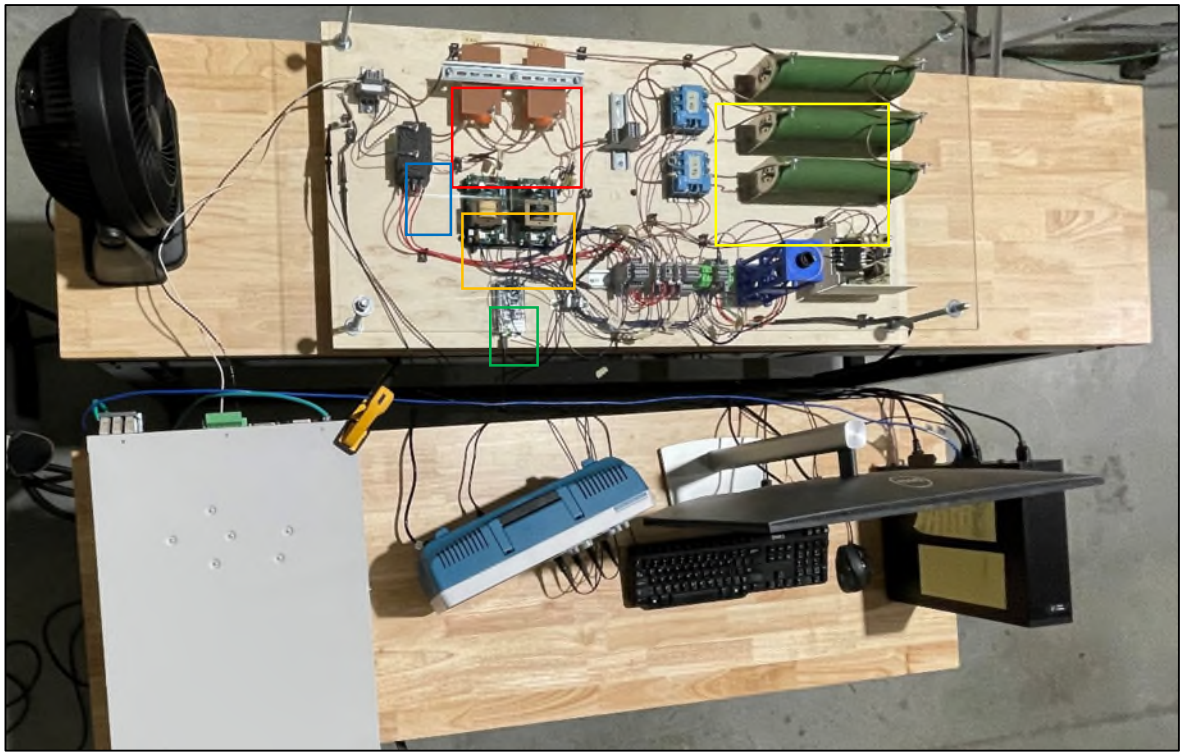

Figure 32. Photo of OVP System test bed with SCRs (red box), gate drivers (orange box), Arduino MCU (green box), DVL 150 voltage sensor (blue box), and load resistors (yellow box).

Figure 33 illustrates the custom voltage processing peripheral circuit that enables the Arduino microcontroller to interface with the rest of the system. The output of the DVL 150 voltage sensor is a 75mA signal corresponding to a voltage measurement of 225V. An appropriately sized resistive shunt is used to convert the current output to a voltage signal between -1.65V and +1.65V. This signal is fed into a non-inverting summing amplifier which serves to add a DC bias of 1.65V, outputting a 0 – 3.3V signal which can be read by the Arduino's integrated 10-bit ADC.

The two outputs of the Arduino, SCR1 and SCR2, control the operation of the gate driver boards. The NPN BJT circuits act as low side switches, impeding the path of the current flowing through the gate driver's input control circuit when the controller detects an over-voltage condition, causing the SCRs to stop conducting at the next current zero-crossing.

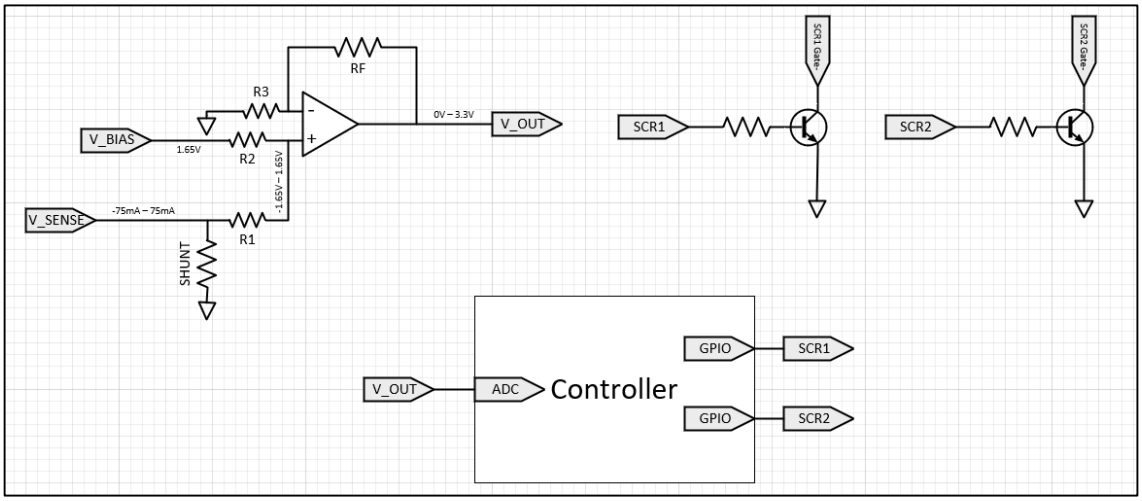

Figure 33. Functional schematic of peripheral circuit used to translate DVL 150 current output signal to 0-3.3V voltage signal to be read by the microcontroller and switch gate drivers on/off.

The control algorithm for the MCU is as follows. The Arduino reads in the "V_OUT" signal through an internal 10-bit analog-to-digital converter (ADC) resulting in a value between 0-1023 (Figure 34). The control algorithm then translates the raw analog value to a voltage as illustrated in the "measureVoltage()" function (Figure 35). Calibration was done to determine the optimal "BIAS" and "GAIN" values to maximize accuracy close to the tripping threshold. The thyristors are commanded to open once the magnitude of a single voltage measurement exceeds the voltage threshold.

```
21 void loop() {
22   voltage = measureVoltage();
23   if (abs(voltage) > OVER_VOLTAGE_THRESHOLD && circuitState == CLOSED)
24   {
25     openThyristors();
26   }
27 }
```

Figure 34. Main control loop algorithm. Following setup, this function repeats indefinitely – polling the ADC and opening the thyristors once voltage rises above the threshold.

```
 7 inline float measureVoltage()
 8 {
 9   int analogValue = analogRead(V_SENSE);
10   float measuredVoltage = analogValue * (3.3 / 1023);
11   return (measuredVoltage - BIAS) / GAIN;
12 }
```

Figure 35. measureVoltage() function used to convert raw ADC output to measured voltage.

The goal of the testing was to subject the OVP system to a scaled version of StingRAY wave data and check that it disconnected the load at the appropriate voltage. Rather than use sine wave data for this experiment, we used a scaled version of the voltage from the model described in Section 6 where the PMG speed input was from C-Power-provided wave-generated velocity data from N7638cs81.mat, which is the highest velocity case in [1]. One phase of the voltage output is shown in Figure 36. The entire data set would be too large to reproduce with the power source so only the worst-case portion of the data from 56 to 59 seconds (Figure 37) was emulated by the power source. Because of power source voltage limitation, we scaled the voltage shown in Figure 37 to align with the limits of the demonstration hardware.

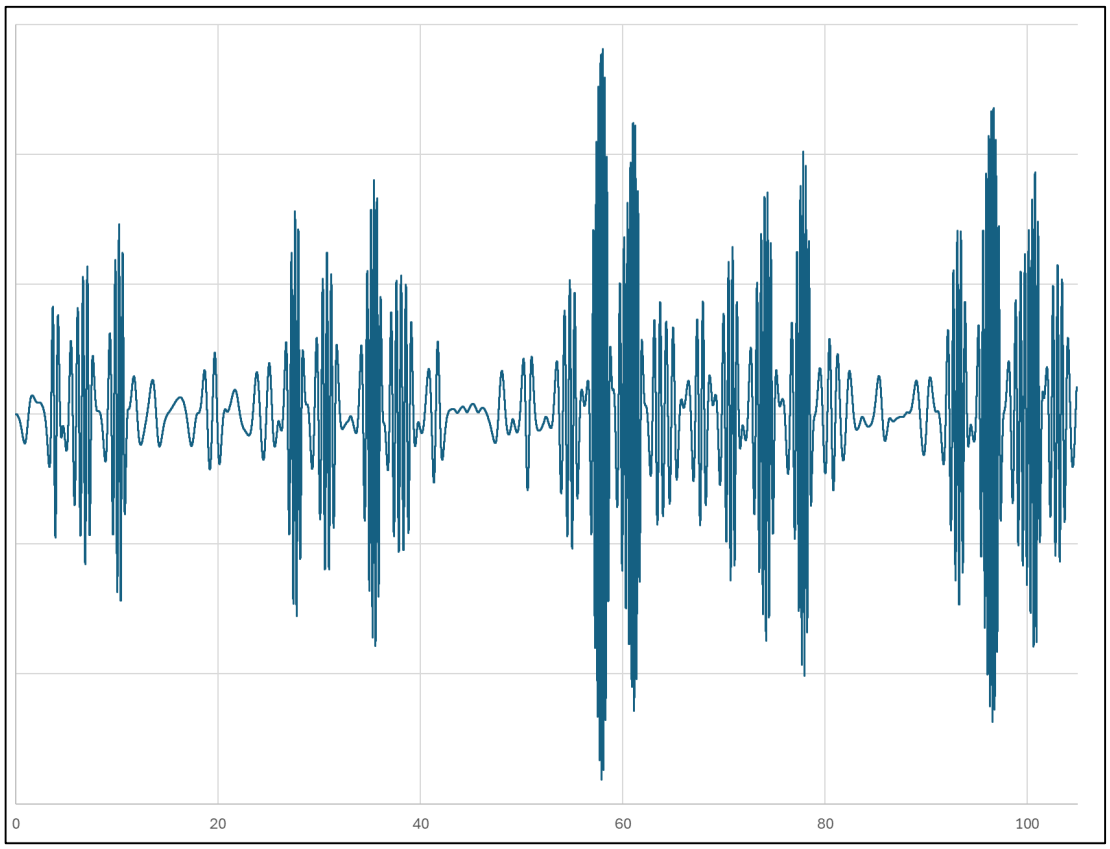

Figure 36. Voltage output from a simulation that uses the worst-case wave data as speed input data.

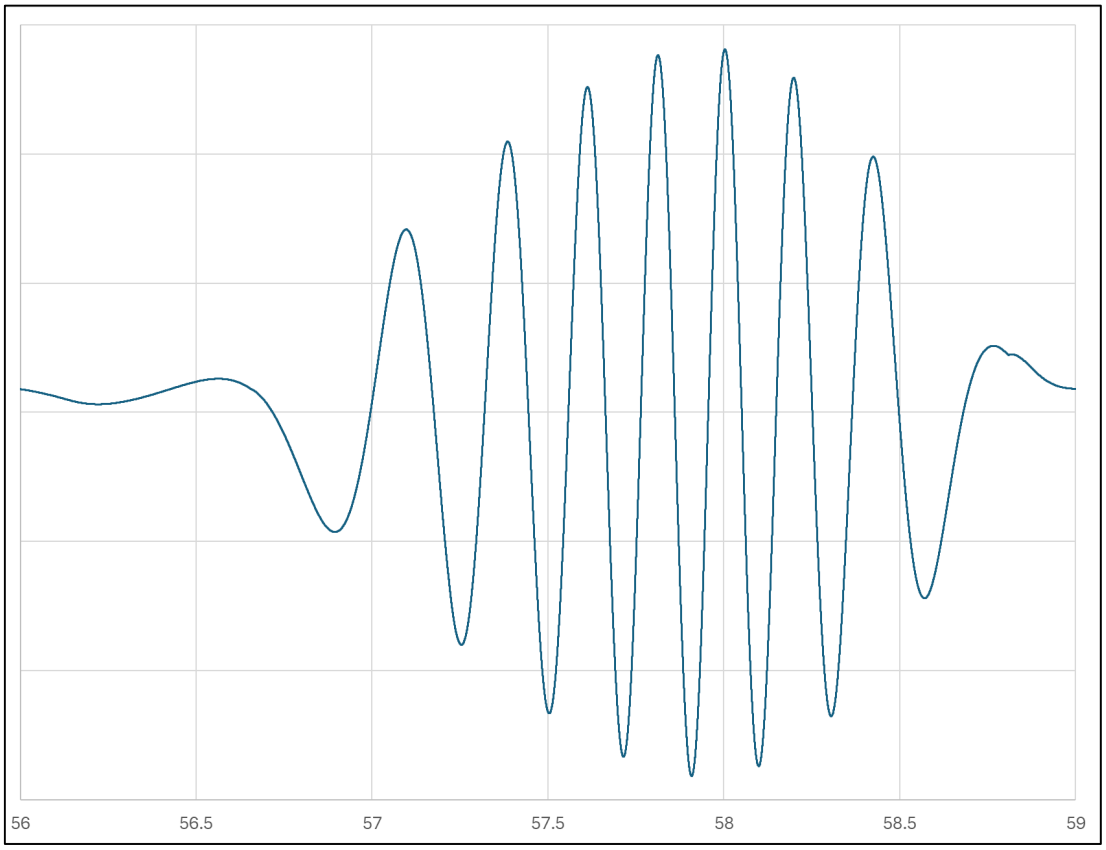

Figure 37. Worst-case voltage output from a simulation that uses the worst-case wave data as speed input data.

The Power Pacific Power 360AFX-2AG was chosen for this project because of its ability to emulate low frequency AC waveforms using its transient sequence function in STEP and RAMP mode as described in [10].

The transient sequence function allows the user to specify 200 voltage points that the supply would iterate through along with the ramp and dwell times. To generate a waveform, we used the provided sea state data as a velocity profile to the model and exported the voltage output of the generator block. Prior to programming the supply, we needed to down-sample the signal given the 200-point limit of the power supply. To maintain the greatest fidelity of the signal – especially at peaks and troughs – a MATLAB script was developed to dynamically adjust the sampling rate based on the magnitude of the second derivative. Using this process, we achieve greater resolution at the inflection points of the wave data. The original and down-sampled voltage data is shown in Figure 38. Note the density of sample points at the peaks and troughs of the waveform. During linear regions of the waveform, the resolution can be lower allowing for more resolution at regions of greater concavity.

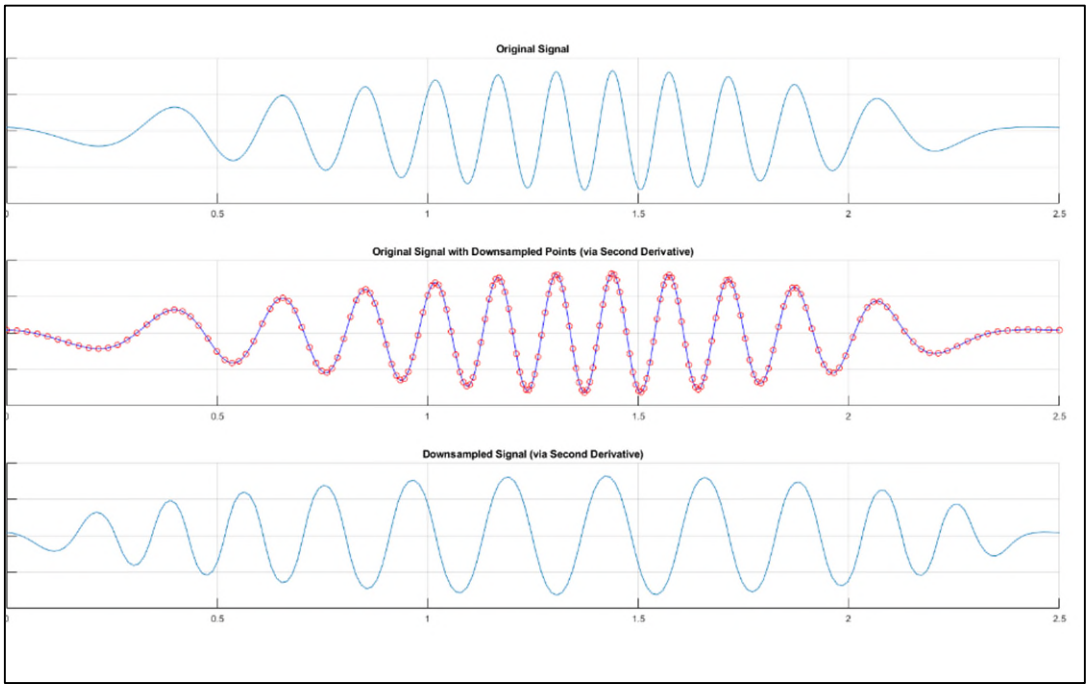

Figure 38. Plot of original (high resolution) waveform (top), sample points (middle) and down-sampled output waveform (bottom).

With the down-sampled signal obtained, the signal was scaled before being programmed into the power supply. For safety and equipment limitations, the experiment was limited to ±150V so the original wave data was scaled down to 150V peak. The same scaling factor was applied to the voltage threshold described below, resulting in a trip threshold of 92V. The scaled voltage as output by the power source is shown in Figure 39.

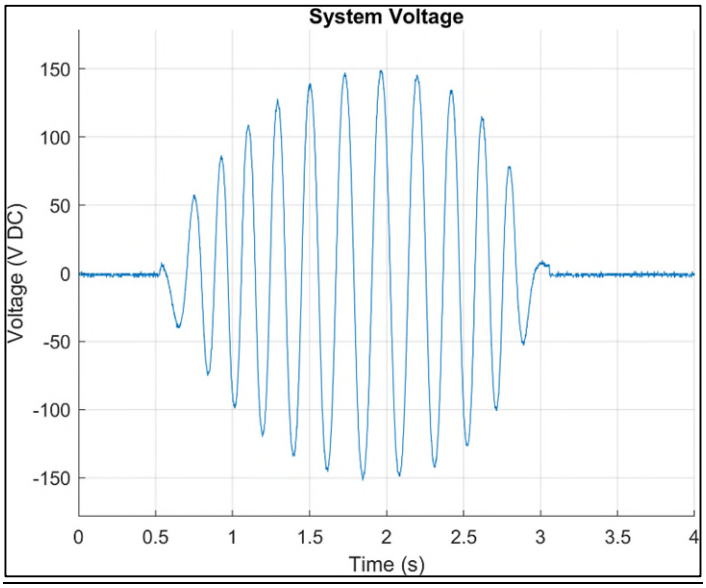

Figure 39. Plot showing the power source's scaled waveform used for the experiment.

Threshold Determination

An important consideration of SCRs is their natural delayed switching behavior. Once the gate is removed, the current through the device must commutate to zero before the device stops conducting. Given the inherent delay of these devices along with the relatively slow frequency of the generator output waveforms, the threshold had to be set low enough that voltage could not rise to an unacceptable level between the time the control gave the disconnect signal and the circuit was interrupted.

As stated previously, the main factor driving the maximum operating voltage of the system is the DC link voltage of the motor drive system. According to [2] and [7], the system can tolerate DC voltages up to 1.09 PU. Based on the assumption that DC link voltage is at minimum 1.35 times the ac line-line voltage (RMS), we arrived at a maximum instantaneous ac voltage (line-line) of 1.61 PU (peak baselined against RMS).

To determine how far in advance protection should be actuated and thus where to set the system's threshold, analysis was done on the provided sea-state data to determine the maximum rate of voltage rise that can be expected. Figure 40 shows a histogram of rates of voltage rise ($\frac{dV}{dt}$) measured from the data at voltages above 1.03 PU along with the associated statistics. We used the 3-sigma value of 0.96PU/s as the maximum rate of voltage rise to be expected. The data consists of all provided sea state data. Noted are the statistics of each dataset (mean, standard deviation, 3-sigma).

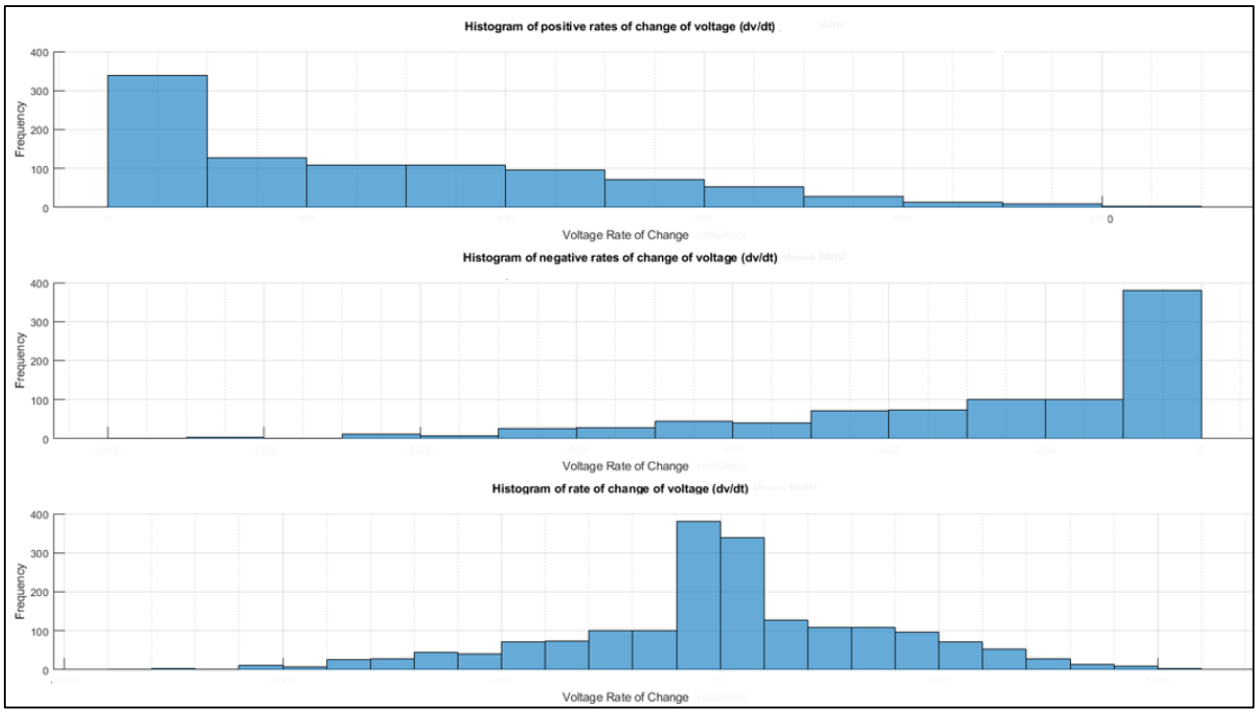

Figure 40. Histogram of rate of voltage rise (top), fall (middle), and rise and fall (bottom) when generator output voltage is at or above 1.03 PU.

If voltage is only being measured on one of the phases of the 3-phase system, at worst-case, one phase would have just experienced a current zero-crossing when an over-voltage condition is observed, yielding

a worst-case delay of ½ the period of the generator output signal. At these voltage levels, the generator output signal has a frequency of about 5 Hz or a period of .2 secs, leading to a maximum delay of .1 secs. The detection and actuation time will occur in less than 1 millisecond to the overall detection to interruption time can be taken as ~0.1 secs. Having determined the maximum operating voltage, maximum rate of voltage rise to be expected, and the worst-case delay time, an optimal tripping threshold was determined to be 1.07 PU (peak compared to rated peak generator output).

Ultimately, we used a threshold of 0.91 PU instantaneous to provide for an additional margin of error.

Once the circuit described above was built and commissioned, the MCU programmed, the data acquisition system configured, and the power source programmed with the waveform shown in Figure 39, we subjected the OVP system to the simulated PMG voltage output.

On the test setup, with the trip threshold voltage set at 92V, the control system compared the absolute value of the AC voltage waveform to the trip threshold and produced a trip at an instantaneous at 89.6V as measured by the oscilloscope (Figure 41), an error of 2.5%. It is not clear whether this error is the result of voltage measurement errors within the control system, within the Hall effect sensor, or within the oscilloscope and probes. A production system would be calibrated to get rid of such errors, but this does demonstrate that the OVP can respond to the input voltage and produce a trip signal.

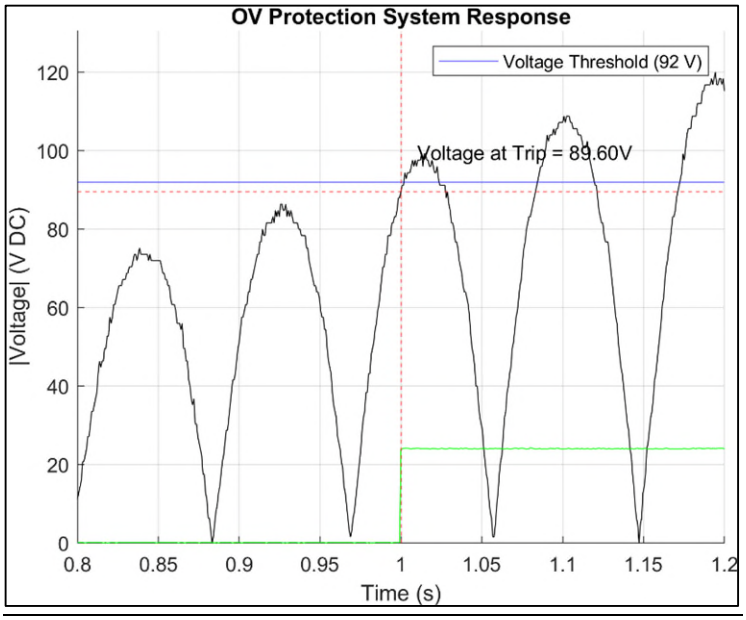

Figure 41. OVP control system's response (green plot) to detection of an over-voltage condition.

Figure 42 and Figure 43 show the voltage seen by the load during the sequence described above. The trip threshold is reached shortly before the voltage peak of the negative-going voltage waveform. At this point, the gate drive current would be removed from the anti-parallel SCRs. Because the conducting SCR continues to conduct until the current zero crossing, the voltage on the load continues to rise, eventually reaching 97.6V before fully commutating off. This indicates that the trip threshold should account for the additional voltage rise that may occur after the trip command is issued.

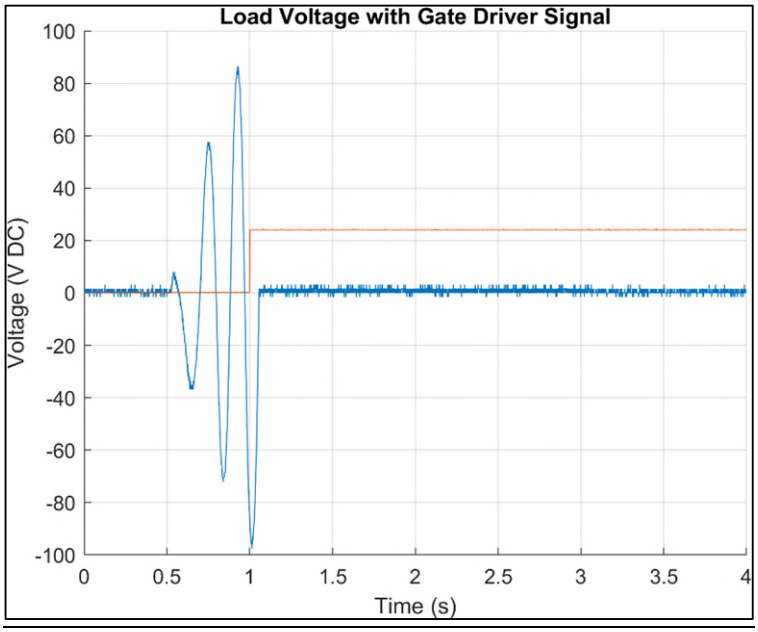

Figure 42. Plot showing the voltage seen by the load which represents the AFE rectifier input.

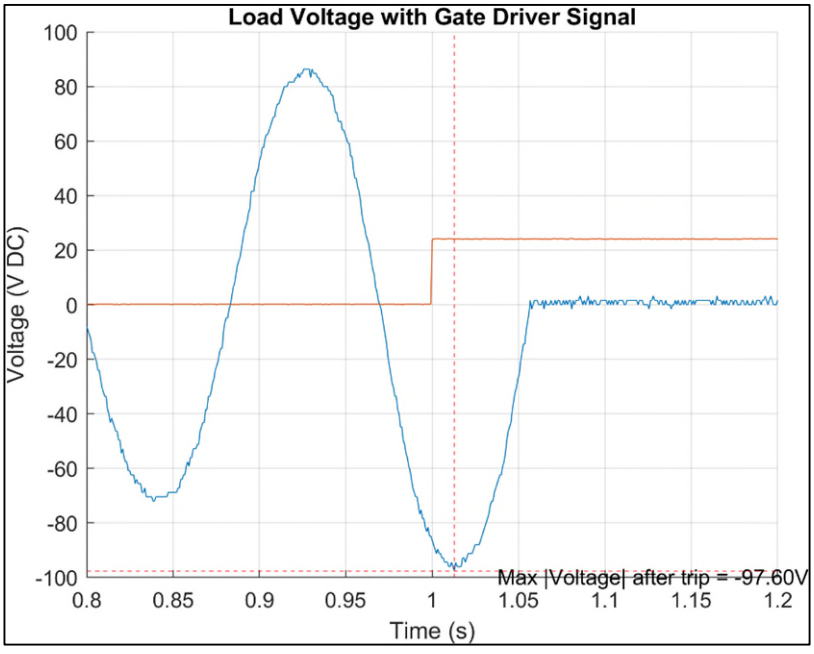

Figure 43. Magnified view of the plot above, noting peak voltage reached.

We consistently observed a discrepancy between the threshold voltage and the measured voltage at the point of trip when using waveforms derived from the wave-data – even after adjusting the tripping threshold to emulate different rates of voltage rise. We did not observe the same discrepancy during calibration or when using constant DC signals or ramp signals. This would be straightforward to troubleshoot and rectify in a production system. At a minimum, the trip threshold should be a user tunable

parameter so that a level can be selected that prevents excessive DC link voltage while avoiding unnecessary nuisance trips.

Although further work needs to be done to develop a more robust control algorithm, the results show that even a low cost MCU based system can successfully monitor the output voltage of a generator in real time and provide the appropriate control response to a switching device in the case of an over-voltage condition. Additionally, we quantified the switching behavior of the thyristor devices, emphasizing the importance of determining the optimal threshold given the inherent switching delays of the system.

We did not implement the algorithm that would be required to reengage the load after the wave causing the trip had passed. For example, this would involve reapplying the gate signal to the thyristors at 3 seconds in Figure 39. This would be relatively easy to implement in a proper industrial controller.

7.2 Optimization Impact Metrics

7.2.1 Power Performance

The effectiveness of the different approaches to reducing overvoltage at improving the key metric of Power Performance (percent improvement in annual mean electrical power at PWS) was assessed as described below.

We first assessed the effects of the increases in trip levels that the proposed OVP methods provide against the generator speed input from the MATLAB data set consisting of 24 different operational sea state simulations with representative annual occurrence rates (data was extrapolated over 8766 hours in a year). This analysis assumes that, once an over-voltage trip occurs, the PMG will remain disconnected from the AFE rectifier until the voltage decreases to less than 50V. Per Table 4, the annual number of trip events where the disconnect switch is activated to take the system offline reduces from 26,534 for the baseline case of 7.61 RPM to 10,778 for the 8.5 RPM case. This is further reduced to 2,457 trips for the case with flux weakening (10 RPM).

Table 4. Number of DC link over-voltage trip events in PWS MATLAB wave data for baseline (7.61 RPM), model with DBC and BESS (8.5 RPM), and model with (10 RPM) flux weakening.

Dataset		7.61 RPM Trip			8.5 RPM Trip			10 RPM Trip		
	Dataset Percent Occurrence per year	Dataset number trip events	Dataset number trips/hour	Dataset number trips/year	Dataset number trip events	Dataset number trips/hour	Dataset number trips/year	Dataset Number trip events	Dataset number trip/hour	Dataset number trips/year
N7638cs3	1.51%	0	0.0	0	0	0.0	0	0	0.0	0
N7638cs9	6.45%	0	0.0	0	0	0.0	0	0	0.0	0
N7638cs15	3.28%	0	0.0	0	0	0.0	0	0	0.0	0
N7638cs21	0.20%	0	0.0	0	0	0.0	0	0	0.0	0
N7638cs27	14.07%	0	0.0	0	0	0.0	0	0	0.0	0
N7638cs33	2.74%	0	0.0	0	0	0.0	0	0	0.0	0
N7638cs39	13.19%	0	0.0	0	0	0.0	0	0	0.0	0
N7638cs45	16.29%	0	0.0	0	0	0.0	0	0	0.0	0
N7638cs51	8.14%	0	0.0	0	0	0.0	0	0	0.0	0
N7638cs57	0.28%	0	0.0	0	0	0.0	0	0	0.0	0
N7638cs63	3.16%	6	9.0	2496	2	3.0	832	1	1.5	416
N7638cs69	10.95%	0	0.0	0	0	0.0	0	0	0.0	0
N7638cs75	3.72%	0	0.0	0	0	0.0	0	0	0.0	0
N7638cs81	0.82%	39	58.6	4236	26	39.1	2824	2	3.0	217
N7638cs87	3.37%	12	18.0	5325	3	4.5	1331	0	0.0	0
N7638cs93	6.32%	2	3.0	1662	0	0.0	0	0	0.0	0
N7638cs99	0.56%	0	0.0	0	0	0.0	0	0	0.0	0
N7638cs105	1.54%	29	43.8	5923	13	19.6	2655	3	4.5	613
N7638cs111	1.65%	3	3.9	558	0	0.0	0	0	0.0	0
N7638cs117	0.42%	8	60.4	2250	5	37.7	1406	3	22.6	844
N7638cs123	0.76%	26	39.1	2590	9	13.5	897	3	4.5	299
N7638cs129	0.22%	2	2.3	43	0	0.0	0	0	0.0	0
N7638cs135	0.21%	9	54.1	1006	5	30.1	559	0	0.0	0
N7638cs141	0.15%	26	33.5	446	16	20.6	274	4	5.1	69
Total number trip events	100.00%			26534			10778			2457

We then performed analysis of the PWS wave data [1] to determine how implementation of standard OVP mitigation methods of DBC plus BESS power flow (which raise the trip threshold to 8.5 RPM), flux weakening (which raises the trip threshold to 10 RPM), and the use of a fast-acting disconnect switch affected the annual mean electrical power as compared to the baseline case where the system trips at 7.61 RPMs and remains offline for 30 seconds and as compared to the ideal situation where no trips occurred.

Assumptions for this analysis were as follows:

- The conventional mechanical circuit breaker, once opened due to an over-voltage event, would remain offline for 30 seconds to allow for spring recharging and reclosing at a trough in output voltage.
- The fast-acting disconnect switch, once opened due to an over-voltage event, would remain offline until generator voltage dropped below 50 volts, at which point it would reclose.
- Loss characterization of the solid-state disconnect switch was based upon a two-leg implementation [4] of antiparallel Hitachi/ABB 5STP2800 thyristors [5]. This design and the loss calculations will be described in greater detail later in this report.
- The analysis does not account for downtime for maintenance or other unscheduled outages and their impact on the mean-time-to-failure (MTTF) of the system. Each loaded switching event for

a conventional mechanical circuit breaker takes life out of the breaker. The downtime to replace or repair a worn out circuit breaker would reduce delivered energy far more than the 30-second interruptions to reconnect to the system. Additionally, every over-voltage event poses a risk to damage components connected to the DC link, particularly DC link capacitors.

The different scenarios are compared to determine how much energy is lost due to over-voltage trips with and without built-in OVP mechanisms (DBC, BESS), with and without flux weakening (FW), how much is lost when accounting for 30 second downtime with a conventional breaker, and how much is lost due to solid-state disconnect switch conduction losses. Results are shown in Table 5.

Comparing the results from the different OVP methods to the 7.6 RPM baseline, we get the following percentage improvements in annual MEP:

- Increasing the trip threshold to 8.5 RPM via DBC and BESS results in a 3.12% increase in MEP versus baseline.
- Further increasing the trip threshold to 10 RPM via FW results in a 5.41% increase in MEP versus baseline.
- Incorporation of a low-loss, fast-acting disconnect switch raises the advantage over baseline for the 10 RPM case to 5.76%
- If the fast-acting disconnect switch is solid-state, the advantage over baseline lowers to 4.71%.

Notable observations from this table regarding comparison to the ideal case with no over-voltage trips:

- The baseline case, with its low trip threshold and 30 second downtime, results in an annual mean electrical power (MEP) reduction of 5.77% versus the ideal case with no trips.
- Simply raising the trip threshold to 8.5 RPM lowers the reduction versus ideal to 2.83%.
- Further raising the trip threshold to 10 RPM via flux weakening changes the reduction versus ideal to 0.68%.
- Implementation of a low-loss fast-acting disconnect switch without conduction losses that reconnect the PMG to the AFE rectifier at an AC voltage less than 50V reduces losses versus ideal to 0.08%.
- If the fast-acting disconnect switch is a solid-state SCR-based switch, losses versus ideal increase to 1.33% with FW. Solid-state disconnect switch SCR losses alone are approximately 1.26% of the ideal delivered energy.

Table 5. Assessment of improvement to annual MEP from incorporation of improved OVP methods

runName	Dataset Percent Occurrence per year	Case 1. Ideal All Energy Available	Case 2. Baseline (7.61 RPM) with 30 s recovery	Case 3. 8.5 RPM, 30s recovery	Case 4. 10 RPM (FW),30s recovery	Case 5. 10 RPM (FW), 50V recovery	Case 6. 10 RPM (FW), 50V recovery with SCR losses
		MEP	MEP	MEP	MEP	MEP	MEP
N7638cs105	**1.54%**	2.34E+05	1.62E+05	1.90E+05	2.22E+05	2.33E+05	2.31E+05
N7638cs111	**1.65%**	1.25E+05	1.21E+05	1.25E+05	1.25E+05	1.25E+05	1.24E+05
N7638cs117	**0.42%**	2.27E+05	1.51E+05	1.74E+05	1.95E+05	2.22E+05	2.20E+05
N7638cs123	**0.76%**	2.01E+05	1.54E+05	1.77E+05	1.94E+05	1.99E+05	1.98E+05
N7638cs129	**0.22%**	1.47E+05	1.44E+05	1.47E+05	1.47E+05	1.47E+05	1.45E+05
N7638cs135	**0.21%**	2.32E+05	1.49E+05	1.76E+05	2.32E+05	2.32E+05	2.30E+05
N7638cs141	**0.15%**	2.03E+05	1.49E+05	1.69E+05	1.93E+05	2.01E+05	2.00E+05
N7638cs15	**3.28%**	1.59E+04	1.59E+04	1.59E+04	1.59E+04	1.59E+04	1.54E+04
N7638cs21	**0.20%**	6.15E+03	6.15E+03	6.15E+03	6.15E+03	6.15E+03	5.79E+03
N7638cs27	**14.07%**	4.81E+04	4.81E+04	4.81E+04	4.81E+04	4.81E+04	4.72E+04
N7638cs3	**1.51%**	3.65E+04	3.65E+04	3.65E+04	3.65E+04	3.65E+04	3.57E+04
N7638cs33	**2.74%**	1.22E+05	1.22E+05	1.22E+05	1.22E+05	1.22E+05	1.21E+05
N7638cs39	**13.19%**	9.84E+04	9.84E+04	9.84E+04	9.84E+04	9.84E+04	9.72E+04
N7638cs45	**16.29%**	6.39E+04	6.39E+04	6.39E+04	6.39E+04	6.39E+04	6.29E+04
N7638cs51	**8.14%**	3.76E+04	3.76E+04	3.76E+04	3.76E+04	3.76E+04	3.68E+04
N7638cs57	**0.28%**	1.98E+04	1.98E+04	1.98E+04	1.98E+04	1.98E+04	1.93E+04
N7638cs63	**3.16%**	1.79E+05	1.59E+05	1.72E+05	1.74E+05	1.79E+05	1.77E+05
N7638cs69	**10.95%**	1.25E+05	1.25E+05	1.25E+05	1.25E+05	1.25E+05	1.24E+05
N7638cs75	**3.72%**	5.75E+04	5.75E+04	5.75E+04	5.75E+04	5.75E+04	5.66E+04
N7638cs81	**0.82%**	2.40E+05	1.46E+05	1.70E+05	2.34E+05	2.40E+05	2.38E+05
N7638cs87	**3.37%**	1.84E+05	1.53E+05	1.73E+05	1.84E+05	1.84E+05	1.82E+05
N7638cs9	**6.45%**	2.84E+04	2.84E+04	2.84E+04	2.84E+04	2.84E+04	2.78E+04
N7638cs93	**6.32%**	1.19E+05	1.13E+05	1.19E+05	1.19E+05	1.19E+05	1.18E+05
N7638cs99	**0.56%**	7.85E+04	7.85E+04	7.85E+04	7.85E+04	7.85E+04	7.74E+04
Annual MEP		8.64E+04	8.15E+04	8.40E+04	8.59E+04	8.64E+04	8.53E+04
MEP increase versus Baseline		+ 6.13%	+ 0.00%	+ 3.12%	+ 5.41%	+ 5.76%	4.71%
MEP decrease versus Ideal		- 0.00%	- 5.77%	- 2.83%	- 0.68%	- 0.08%	- 1.33%

The method of determining annual MEP for the cases above was as follows:

- Ideal, with no trips occurring. This is not realistic but shows the maximum Mean Electrical Power (MEP) that could be delivered annually [1] if no trip occurred. The energy for the dataset is integrated and converted to an MEP for the specific dataset, which is then converted to an hourly MEP based upon the length of the dataset. The hourly MEPs for specific datasets along with dataset annual occurrence rates are used to calculate the annual MEP.
- Baseline case from original data with a trip threshold of 7.61 RPM. Similar to the above case, the energy for the data is integrated but the 30 second off time between the point at which the switch opens and when it recloses is omitted from the integration.
- Case with no flux weakening from simulation with an over-voltage trip of 8.5 RPM, and with a slow-acting circuit breaker with 30 seconds recovery for each trip. This is from simulation results and accounts for the effects of the DBC, BESS, and energy output to the grid on lowering DC link

voltage. It also accounts for voltage drops across system impedances. Similar to the above case, the energy for the data is integrated but the off time between the point at which the switch opens and when it recloses is omitted from the integration.

- Flux weakening, resulting in over-voltage trips at 10 RPM, and with a slow-acting circuit breaker with 30 seconds recovery for each trip. Similar to the above cases, the energy for the data is integrated but the off time between the point at which the switch opens and when it recloses is omitted from the integration.
- Flux weakening with a fast-acting, low-loss mechanical switch, described in 7.3, that trips upon over-voltage at 10 RPMs then reconnects when voltage drops below 50V. The energy for the data is integrated but the off time between the points at which the switch opens and when it recloses is omitted from the integration.

Flux weakening, resulting in over-voltage trips at 10 RPM, and with a fast-acting solid-state switch with representative losses for a solid-state switch as shown in Figure 45 below. The losses were calculated by taking the results in Case 2 (flux weakening with low-loss, fast-acting switch) and multiplying them by the calculated efficiency of the solid-state switch at the average current for each of the runs described in [1]. This efficiency is calculated by finding the average power for each of the runs, determining the RMS current for the run, calculating the average current per SCR, then determining the individual SCR loss for that average current using datasheet parameters. This average loss is then multiplied by four to account for the four SCRs in the switch. Control system losses are assumed to be 100W. These losses and the average power for the run are used to calculate an efficiency for that run, which is applied to the Case 2 data to get the total energy for the SCR-based switch. The results of this analysis are shown in Table 6.

Table 6. SCR-based disconnect switch losses for individual runs and resulting efficiency

runName	Average Power (kW)	Current from spreadsht	Ave current per SCR	SCR (formula below 180 °	Loss per phase	Loss per 2 phase, W	Assumed control loss , W	Total Switch Losses, W	Efficiency
N7638cs105	234.39	870	391.64	418.01786	836.0357	1672.071	100	1772.071	0.9924397
N7638cs111	125.46	683	307.46	313.80371	627.6074	1255.215	100	1355.215	0.9891985
N7638cs117	227.49	870	391.64	418.01786	836.0357	1672.071	100	1772.071	0.9922104
N7638cs123	200.63	870	391.64	418.01786	836.0357	1672.071	100	1772.071	0.9911675
N7638cs129	146.85	765	344.37	358.53356	717.0671	1434.134	100	1534.134	0.9895534
N7638cs135	231.55	870	391.64	418.01786	836.0357	1672.071	100	1772.071	0.992347
N7638cs141	202.64	870	391.64	418.01786	836.0357	1672.071	100	1772.071	0.9912552
N7638cs15	15.89	246	110.74	100.93409	201.8682	403.7364	100	503.7364	0.9682903
N7638cs21	6.15	164	73.83	65.776947	131.5539	263.1078	100	363.1078	0.9409833
N7638cs27	48.05	437	196.72	188.68887	377.3777	754.7555	100	854.7555	0.9822116
N7638cs3	36.48	382	171.96	162.57792	325.1558	650.3117	100	750.3117	0.9794307
N7638cs33	122.21	683	307.46	313.80371	627.6074	1255.215	100	1355.215	0.9889107
N7638cs39	98.35	601	270.55	270.58631	541.1726	1082.345	100	1182.345	0.9879785
N7638cs45	63.89	492	221.48	215.48024	430.9605	861.9209	100	961.9209	0.9849441
N7638cs51	37.56	382	171.96	162.57792	325.1558	650.3117	100	750.3117	0.9800211
N7638cs57	19.85	273	122.89	112.84122	225.6824	451.3649	100	551.3649	0.9722169
N7638cs63	178.88	820	369.13	389.38272	778.7654	1557.531	100	1657.531	0.9907339
N7638cs69	125.05	683	307.46	313.80371	627.6074	1255.215	100	1355.215	0.9891626
N7638cs75	57.49	464	208.87	201.75597	403.5119	807.0239	100	907.0239	0.9842224
N7638cs81	240.35	870	391.64	418.01786	836.0357	1672.071	100	1772.071	0.9926271
N7638cs87	184.05	847	381.28	404.77586	809.5517	1619.103	100	1719.103	0.9906596
N7638cs9	28.42	328	147.65	137.60369	275.2074	550.4148	100	650.4148	0.9771175
N7638cs93	119.40	683	307.46	313.80371	627.6074	1255.215	100	1355.215	0.9886501
N7638cs99	78.50	546	245.79	242.44647	484.8929	969.7859	100	1069.786	0.9863729

7.2.2 Capital Expense

As discussed later in 7.3, capital expense for flux weakening would have to be negotiated with the AFE rectifier manufacturer. Capital expense for the fast-acting switch would depend on whether a solid-state or vacuum-contactor disconnect switch was selected. The cost for the solid-state switch is estimated at $30k-50k. The cost for the vacuum-contactor-based disconnect switch is estimated at roughly $16k.

7.2.3 Mean time to failures (MTTF) for the improved OVP system

The proposed design (flux weakening and fast-acting, long-lifetime disconnect switch) will improve MTTF as discussed below.

- Reduced circuit breaker wear and tear. Flux weakening reduces the number of annual trips per year from 26,534 per year to 2,457 trips per year. For a circuit breaker rated at 1,000 loaded switching operations, this would reduce the failure rate from 27 times per year to 2.5 times per year, a roughly 1100% annual improvement. For a circuit breaker rated at 5,000 loaded switching operations, this would reduce the failure rate from 5.3 times per year to 0.49 times per year, also an 1100% improvement.

- Eliminated circuit breaker wear and tear. Replacing the circuit breaker with a solid-state disconnect switch or vacuum contactor as discussed in 7.3 would eliminate circuit breaker wear and tear for the solid-state disconnect switch and would essentially eliminate switch downtime for the vacuum contactor, which is rated at 500,000 loaded operations.
- Reduced exposure to overvoltage events with flux weakening. As noted above, flux weakening reduces the annual number of over-voltage events from 26,534 to 2,457, a roughly 1100% annual improvement. Each of these events exposes equipment connected to the system's DC link to additional stress. This is of particular concern for DC link capacitors. The improvement can't be easily quantified in terms of improved MTTF.
- Reduced exposure to overvoltage due to faster disconnection. For the solid-state disconnect in particular, the fast opening time will disconnect the AFE rectifier from the PMG faster than a conventional circuit breaker, which will have an opening time of 50-100 ms after which the current will commutate off at a current zero crossing. The voltage continues to rise from the time an over-voltage has been declared until the current commutates off. The longer opening time will allow more time for the voltage to rise, putting equipment connected to the DC link at risk.

7.3 Design Summary

The two modifications of the StingRAY power system recommended in the report are implementation of flux weakening and implementation of a fast-acting switch, long-lifetime switch to take the system offline during impending over-voltages.

7.3.1 Flux weakening design

The design for flux weakening would be implemented within the AFE rectifier controls. This would require coordination with the manufacturer to modify the rectifier controls to implement this feature. As described in Figure 20 and Figure 21, this involves injecting d-axis current when generator speed exceeds 7.35 RPM. During flux weakening, the combination of q-axis current and flux-weakening d-axis current will equate to the maximum generator current. The cost to implement this feature is unknown and would have to be determined through negotiations with the manufacturer.

7.3.2 Disconnect switch design

The original concept for disconnect switch design consisted of a thyristor-based switch similar in concept to one side of a solid-state automatic bus transfer switch (SABT). We had originally planned on use of a Hitachi 5STP 16F2810 rated at 2800V and 1500 A (with forced cooling) but concerns about efficiency caused us to switch to a Hitachi 5STP 33L2800 rated at 2800V and 3740 A average. The 5STP 33L2800 is a 78mm low-loss thyristor that would be mounted to fan cooled heat sink like the assembly shown in Figure 44, modified for a three-phase circuit using a two-leg topology as shown in Figure 45. The two-leg topology is common in three-phase, three-wire SCR applications such as water heaters, soft-starters, and welding power supplies. In addition to the thyristors, heat sinks, gate drives, fans, and system controls; this switch would need an enclosure, buswork, cabling, and other peripheral components. Detailed costs for this switch were not developed but experience with similar systems, such as bus transfer switches, indicates that the cost will be between $30,000 and $50,000 dollars. This cost and additional losses resulting from the use of a solid-state switch (see

Table 6Table 6) would need to be assessed against the potential savings due to decreased downtime.

Figure 44. Three-phase air-cooled thyristor assembly [11]

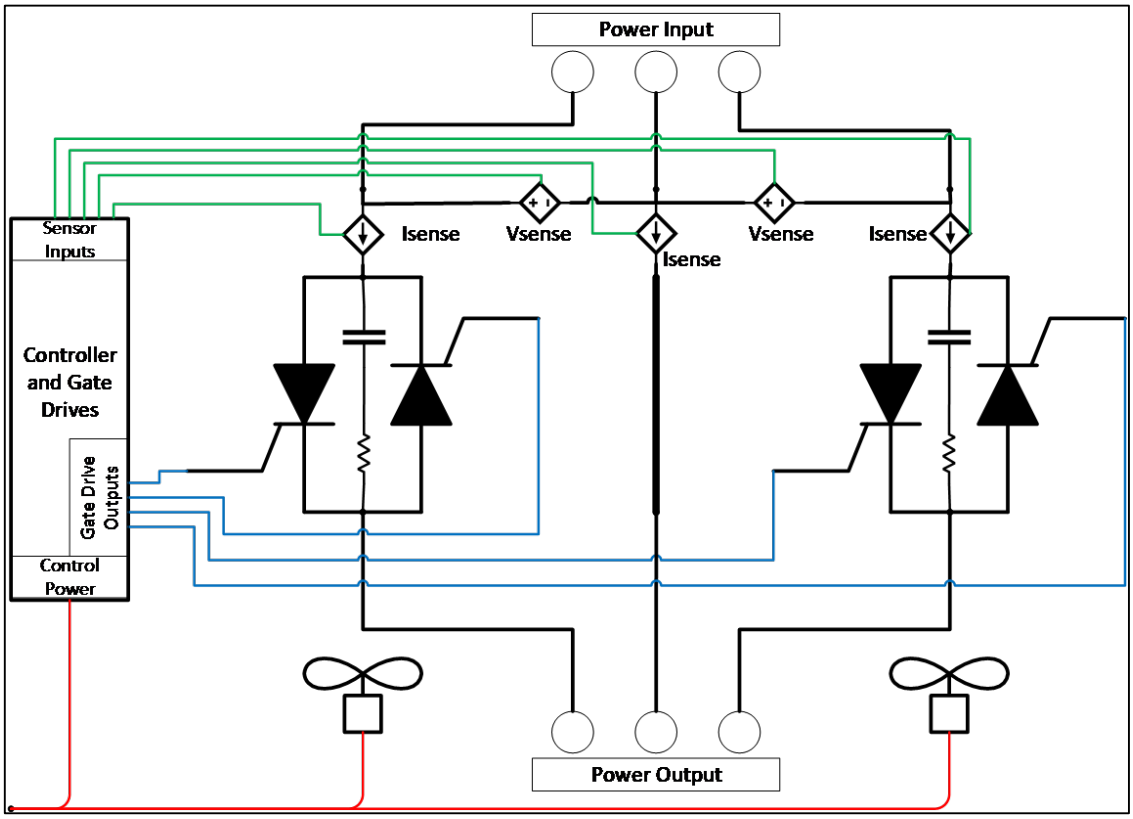

Figure 45. Schematic for SCR-based disconnect switch.

Because of the losses and high cost of the solid-state disconnect switch, we explored mechanical switching options that could achieve the high number of switching cycles needed for remote operation without needing to replace or repair the switch frequently. The best technology we found was low-voltage vacuum contactors. The three most promising options found are all from Joslyn-Clark. These are:

- VC77U03615-76, rated at 1,500V RMS, 600A RMS, and 1,000,000 electrical switching operations
- VC77U03636-76, rated at 3,300V RMS, 600A RMS, and 1,000,000 electrical switching operations
- CV77036A15-76, rated at 1,500V RMS, 600A RMS, and 500,000 electrical switching operations

Because of the 600 A RMS current rating, one switch would be required for each of the two machine AFE rectifiers. Because of its low cost and very compact dimensions, we propose using the VC77U036015-76, shown in Figure 46. These are priced at $5,577 by Joslyn Clark's preferred distributor so two would cost $11,154. Similar Joslyn Clark vacuum contactors have been used with great success in marine use for motor controller and mechanical bus transfer switch (MBT) applications. One example is shown in the right graphic in Figure 46. These would not require cooling or gate drives, unlike the SCR-based switch. They would still need a controller to determine the tripping point. The controller would be simpler than that of the SCR-based switch because it would not need sophisticated gate drives, just a dry contact closure. Estimated cost for the controls and enclosure would be $5000, bringing the total to $16,154 when accounting for the two vacuum contactors.

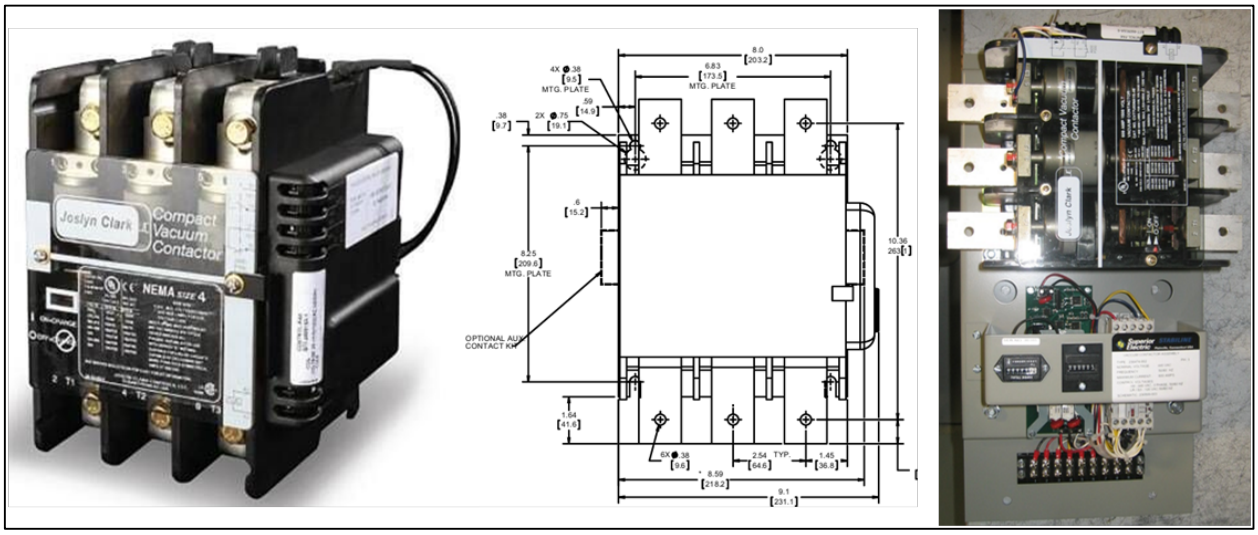

Figure 46. Joslyn Clark VC77U036015-76 1,500 V RMS, 600 A RMS vacuum contactor.

7.4 Lesson Learned and Test Plan Deviation

7.4.1 Lessons Learned

When using modeling and simulation to improve system design, integration, and validation of power electronic components, it is critical to have access to high fidelity models that accurately represent the system and the area of analysis. Additionally, those models must be modeled using the appropriate techniques and be validated to support their intended use especially when power system dynamics are in view. The very nature of this effort was to improve the existing system design and to analyze the efficacy and viability of various protections methods. Without leveraging existing system design component models, developing such a protection scheme required Cardinal Engineering to make assumptions based on common design standards and best practices about the system components and their operation. Modeling efforts undertaken in this effort to evaluate OVP methods took considerable effort taking away time from OVP evaluation and test efforts. Knowing what electrical models were available from OEMs or previously developed before the proposal phase would have greatly improved our methods and test plan development as demonstrated below.

The solid-state disconnect switch has great promise in eliminating circuit breaker wear-and-tear, quickly disconnecting the AFE rectifier from the PMG during impending over-voltages, and quickly reconnecting the AFE rectifier after the over-voltage condition passed. This led us to accept it as the default disconnect switch. However, analysis late in the program showed that use of the solid-state switch yielded losses of 1.25% of total electrical energy generated, giving back many of the gains obtained from reduced off-time. This led to a search for a long-life, low-loss mechanical switch. We found low voltage vacuum contactors to be a very promising option. Discovering this earlier would have allowed more time to optimize this option.

7.4.2 Test Plan Deviations

It was originally conceived that a CHIL test would be performed to allow the OVP controller to operate directly with modeled power system components. Upon analysis of the various OVP methods and modeling activities it was determined that specific implementation of the power electronics and their associated controls is critical to OVP controller design. Although the flux weakening method was of great interest the implementation would be highly dependent on system architecture and the associated production equipment. Implementing a CHIL experiment would not provide additional value or insight beyond the already completed modeling activities. The method of solid-state switch to disconnect the PMG from the AFE rectifier upon detection of a condition that could cause a DC link over-voltage can be used in conjunction with the flux weakening method and would benefit from a hardware-based test. The test outlined in Section 6 used real representative OVP protection hardware (switch & sensor) but with a notional OVP controller. Additionally, the initial implementation of the OVP controller was envisioned to be a PLC, but based on the solid-state switch OVP method, a OVP control algorithm on a PLC would have been overly complex for such a method.

8. Conclusions and Recommendations

8.1 Conclusions

Addition of flux weakening and a fast-acting, solid-state disconnect switch delivers about 4.71% more Mean Electrical Power than the baseline case with a 7.6 RPM trip point and 30 second off time after a trip. This improves to 5.76% higher MEP if a vacuum contactor-based disconnect switch is used.

The addition, this approach greatly improves system MTTF by eliminating trips of the conventional circuit breaker, which degrade its life substantially, potentially resulting in 5.3 failures per year for a circuit breaker rated for 5,000 loaded operations (a typical value). Failures will be more frequent if the circuit breaker is rated for few operations. MTTF will also be improved by reducing system components to overvoltage events in general.

The improved MTTF and additional energy delivered must be balanced against the cost of implementing the improvements. We do not have a cost for implementing flux weakening. This would have to be integrated into the AFE rectifier controls by the OEM. We estimate the cost of the solid-state disconnect switch to be between $30,000 and $50,000. We estimate the cost of the vacuum contactor-based disconnect switch to be approximately $16,000. These costs are trivial in the context of the overall cost of the system.

A complete overvoltage protection system for a direct drive wave power system (WPS) includes normally operating and emergency system components. The baseline design for comparison for this analysis included the emergency system components for protection against over-voltage electrical faults; the dynamics breaking copper (DBC) which protects the DC-link, and the PMG circuit breaker, which protects the entire system in case of a fault or extreme over-voltage event. The normally operating components include inverters to direct current and power flow, and a high-power in-line silicon control rectifier (SCR) to momentarily isolate the generator during normally occurring transient over-voltages. The front-end inverters that control the generator should be designed to include flux-weakening controls which allow

for the injection of off-angle AC current to reduce the generator output terminal voltage. The power conversion system should include inverters coupled to the DC-link that manage power flow between energy storage (ES) and the grid for maximum power conversion efficiency, availability and reliability. These system components are relatively low in cost compared to total WPS CAPEX and would reduce the system MTTF while increasing annual energy production.

8.1.1 StingRAY Modelling conclusions

The results of the model provide a first-order analysis of the efficacy of flux weakening as a DC link over-voltage protection strategy. As the model for the overall control system includes many assumptions, many questions remain regarding the interaction of the various subsystems. For example, it is still unclear the extent that the AFE rectifier control system can be modified, so we would have to work with the Original Equipment Manufacturer (OEM) to determine the practicality of implementing flux weakening. As the design process continues and more details are established, further modeling work should be done in conjunction with the OEM to develop a better understanding of the dynamics of the system and more accurately quantify its operating characteristics.

8.1.2 OVP testing conclusions

Testing of the proposed OVP strategy of disconnecting the PMG from the AFE rectifier demonstrated that a detection algorithm based upon sensing instantaneous absolute voltage is feasible and straightforward to implement. The production system would require fine tuning to select the appropriate trip threshold based on actual StingRAY system behavior. The concept of using an SCR-based switch was verified. Although a production system would differ from the lab-scale OVP, the basic concepts were proven and use of an SCR-based OVP to disconnect during moments of impending DC link over-voltage is a low-risk method of improving StingRAY availability and average power output.

8.2 Recommendations:

8.2.1 Modelling and Flux Weakening Recommendations

- Near-term: When StingRAY is nearing production, work with C-Power and the AFE rectifier OEM to refine the simulation model, making it more reflective of actual control system and hardware behavior.
- Near-term: Work with the AFE rectifier OEM to change AFE rectifier controls to implement flux weakening within the AFE rectifier control in a manner similar to what is shown here.
- Near-term: The system could be made more robust and effective if the trip signal was based upon actual DC link voltage rather than the input AC voltage because the AC input to DC output is calculated and therefore may introduce inaccuracies in the trip settings.
- Longer term: Optimize the BESS controls to draw higher real power during periods of high generator output power or high DC link voltage. By doing this, the BESS could supplement the DBC in voltage regulation.
- Longer term: Optimize the output AFE inverter to use its full rating and the transient rating of the output transformer to provide power to the grid at or above the steady-state rating of the transformer during periods of high generator output power or high DC link voltage. This, too,

could help regulate the DC link voltage in a manner similar to the DBC by drawing higher real power from the DC bus.

- Longer term: Coordinate operation of the BESS with that of the output AFE Inverter to fill in the gaps when generator velocity is low to smooth out the delivered power. This would have a secondary benefit of lowering the BESS battery's state of charge during periods of low RPM so that more energy could be diverted to the battery during periods of high RPM. This would have to be an adaptive algorithm to ensure that the average delivered power from the output AFE inverter matches power produced by the generator when averaged over a sufficient period. The sum of power into and out of the BESS must average to zero in order to maintain overall battery state of charge. For example, if the average power delivered by the output AFE inverter is greater than that of the PMG, the battery will be depleted over time.
- Longer term: Combine mechanical and electrical physics-based modeling and simulation in order to gain a better understanding of the complex interactions between mechanical movement and electrical output.

8.2.2 Testing and OVP recommendations

- Near term: Incorporate a solid-state or vacuum contactor disconnect switch as an OVP device into the StingRAY design. This would enable disconnection and rapid reconnection of the PMG to the AFE rectifier upon detection of events which could cause an over-voltage.
- Near term: Refine controls to improve trip threshold accuracy and to implement a reconnecting function at the bottom of the wave when voltage and speed are near zero.
- Longer term: If the cost and losses of the solid-state disconnect switch are acceptable, develop and test a production-level three-phase OVP device using SCRs that incorporates three-phase SCR switches, a proper industrial-grade control system, thermal management (probably air-cooled finned heat sinks) and packaging.
- Longer term: If a vacuum contactor disconnect switch is preferred, develop and test a complete OV protection system with two vacuum contactor, an industrial-grade control system and packaging.
- Longer term: If StingRAY is slated for production and projects that Cardinal Engineering has in the works to develop a portable power source are funded and completed, conduct testing of the overall StingRAY power system or individual StingRAY components using a portable power source to replicate PMG behavior.

9. REFERENCES

[1] C-Power, *Matlab data OvrVolt_30sep2024.zip,* 2024.

[2] General Electric Company, "USCO-002881 / V08P01C01S1 SingRAY H3 System Overall Report," 2022.

[3] General Electric Company, "DOC0089145 PM Generator Datasheet & Characteristic Curves, GE Confidential," 2022.

[4] Watlow Electric Manufacturing Company, "The benefits of two-leg versus three-leg power control, in three phase heating applications, Document number HA032954 Issue 2," 2023.

[5] Hitachi Energy Ltd, "Phase Control Thyristor 5STP33L2800 datasheet, Document number 5SYA11011-07 May 20," 2020.

[6] V. Patel, General Electric Company, *CY20381-EfficiencyMapCalculation_JP2024_master.xlsm,* 2024.

[7] GE Vernova, *Brochure GEA34922 LV3 DMR 1250A PECe,* 2024.

[8] Avid Controls Inc., "DTS-01353-CUS-A-REV_01 GDB400-4705-A 400A Dynamic Braking Unit - User Manual," 2018.

[9] Sanil Electric Co. Ltd., *Dry Type Transformer Technical Data Sheet SM21145 dated 29 October 2021.*

[10] Pacific Power Source, Inc., *Operation Manual, AFX Series - Rev 1.4.0,* 2024.

[11] "https://www.appliedps.com/power-semiconductor-assemblies," Applied Power Systems Incorporated. [Online].